Measurement report: Stoichiometry of dissolved iron and aluminum as an indicator of the factors controlling the fractional solubility of aerosol iron: Results of the annual observations of size-fractionated aerosol particles in Japan

Kohei Sakata[1*], Aya Sakaguchi[2], Yoshiaki Yamakawa[3], Chihiro Miyamoto[3], Minako Kurisu[4], Yoshio Takahashi[3]

[1]Earth System Division, National Institute for Environmental Studies, 16-2 Onogawa, Tsukuba, Ibaraki 305-8506, Japan

[2]Institute of Pure and Applied Science, University of Tsukuba, 1-1-1 Tennodai, Tsukuba, Ibaraki 305-8577, Japan

[3]Graduate School of Science, the University of Tokyo, 7-3-1 Hongo, Bunkyo-ku, Tokyo, 113-0033, Japan

[4]Research Institute for Marine Resources Utilization, Japan Agency for Marine-Earth Science and Technology, 2-15 Natsuhshima-cho, Yokosuka, Kanagawa 237-0061, Japan

Correspondence to: Kohei Sakata (sakata.kohei@nies.go.jp)

Abstract.

The atmospheric deposition of iron (Fe) promotes primary production in the surface ocean, which results in the enhanced uptake of carbon dioxide into surface seawater. Given that microorganisms in seawater utilize dissolved Fe (d-Fe) as a nutrient, the bioavailability of Fe in aerosol particles depends on its solubility. However, the factors controlling fractional Fe solubility (Fe_{sol}%) in aerosol particles have not been fully understood. This study performed annual observations of the total and dissolved metal concentrations in size-fractionated (seven fractions) aerosol particles at Higashi-Hiroshima, Japan. The feasibility of the molar concentration ratio of d-Fe relative to dissolved Al ([d-Fe]/[d-Al]) as an indicator of sources of d-Fe in aerosol particles was investigated because this ratio is likely dependent on the emission sources of Fe (e.g., mineral dust, fly ash, and anthropogenic Fe oxides) and their dissolution processes (proton- and ligand-promoted dissolutions). Approximately 70 % of the total Fe in total suspended particulate (TSP) were present in coarse aerosol particles, whereas about 70% of d-Fe in TSP were mainly found in fine aerosol particles. The average Fe_{sol}% in fine aerosol particles (11.4 ± 7.0 %) was higher than that of coarse aerosol particles (2.19 ± 2.27%). In addition, the average ratio of [d-Fe]/[d-Al] in coarse aerosol particles (0.408 ± 0.168) was lower than that in fine aerosol particles (1.15 ± 0.80). The range of [d-Fe]/[d-Al] ratios in the coarse aerosol particles (0.121–0.927) was similar to that obtained by proton-promoted dissolution of mineral dust (0.1–1.0), which indicates that the d-Fe in coarse aerosol particles was derived from mineral dust. The [d-Fe]/[d-Al] ratios of fine aerosol particles ranged from 0.386 to 4.67, and [d-Fe]/[d-Al] ratios greater than 1.50 cannot be explained by proton- and ligand-promoted dissolutions ($1.00 < [d\text{-}Fe]/[d\text{-}Al] < 1.50$). The [d-Fe]/[d-Al] ratio correlated with the enrichment factor of Fe in fine aerosol particles (r: 0.505), which indicates that anthropogenic Fe with a high [d-Fe]/[d-Al] ratio was the source of d-Fe in fine aerosol particles. The high [d-Fe]/[d-Al] ratio was attributed to anthropogenic Fe oxides emitted from high-temperature combustions. Finally, the fraction of anthropogenic Fe oxides to d-Fe in total suspended particulate (TSP) was calculated based on the [d-Fe]/[d-Al] ratio of aerosols and their emission source samples. As a result, the fraction of anthropogenic Fe oxides to d-Fe in TSP varied from 1.48 % to 80.7 %. A high fraction was observed in summer when air masses originated from industrial regions in Japan. By contrast, approximately 10 % of d-Fe in the TSP samples collected in spring and during Asian dust events was derived from anthropogenic Fe oxides when air masses frequently transported from East Asia to the Pacific Ocean. Thus, mineral dust was the dominant source of d-Fe in Asian outflow to the Pacific Ocean.

1. Introduction

Primary production in high-nutrient low-chlorophyll regions, such as the North Pacific, Eastern Equatorial Pacific, and Southern Ocean, is limited by the depletion of dissolved Fe (d-Fe, Martin and Fitzwater, 1988; Boyd et al., 2007; Moore et al., 2013; Tagliabue et al., 2017). The atmospheric deposition of Fe activates primary productions in surface seawater, which enhances the oceanic uptake of atmospheric CO_2 (Martin, 1990; Martin et al., 1994; Falkowski et al., 2000; Jickells et al., 2005). In the last glacial–interglacial period, the atmospheric CO_2 concentration was inversely correlated with the supply of mineral dust to the Southern Ocean (Martínez-Garcia et al., 2009, 2011, 2014). Thus, the fertilization of d-Fe in surface seawater via aerosol deposition is an important driver of the global climate system. Given that phytoplankton in surface seawater utilizes d-Fe as nutrient, the bioavailability of Fe in aerosol particles depends on its solubility (Moore et al., 2013). Iron in aerosols has low solubility in water, and the solubility of fractional Fe (Fe_{sol}% = (d-Fe/total Fe) × 100) in marine aerosols ranges from 0.1 % to 90 % (Sholkovitz et al., 2012; Mahowald et al., 2018). Factors controlling Fe_{sol}% include the differences in the Fe_{sol}% among emission sources (e.g., mineral dust versus anthropogenic aerosol) and atmospheric processes of Fe-bearing particles (Sedwick et al., 2007; Sholkovitz et al., 2009; Mahowald et al., 2018; Ito et al., 2019, 2021). In addition, previous studies revealed that the factors have size dependences because fine aerosol particles yield higher Fe_{sol}% than coarse aerosol particles derived from either or both anthropogenic Fe and atmospheric processes (Buck et al., 2010a; Chance et al., 2015; Sakata et al., 2018; Kurisu et al., 2021; Baker and Jickells, 2006, 2017; Baker et al., 2020; Gao et al., 2019). However, the factors controlling Fe_{sol}% in aerosol particles have not been fully understood.

Source apportionment of d-Fe in aerosol particles has been conducted based on the correlation analysis of Fe_{sol}% with the concentrations and enrichment factors (EFs) of coexisting elements. The EFs of vanadium (V) and lead (Pb) are used as tracer elements of heavy-oil and coal combustion processes, respectively (Sholkovitz et al., 2009; Conway et al., 2019; Hsieh et al., 2022). The correlations of Fe_{sol}% with the EFs of V and Pb are useful for evaluating the presence of anthropogenic Fe. However, quantitative evaluation of the fraction of anthropogenic Fe in d-Fe in aerosol particles is difficult. Therefore, an indicator that can estimate the fraction of anthropogenic Fe in d-Fe in aerosols is required to evaluate quantitatively the Fe supply from aerosols to the ocean surface. The fraction of anthropogenic Fe was recently estimated using the Fe isotope ratio (δ^{56}Fe); anthropogenic Fe has a lower δ^{56}Fe than mineral dust (Kurisu et al., 2016a and b, 2019, 2021; Conway et al., 2019). Although the δ^{56}Fe of total Fe in marine aerosol particles has been reported by previous studies, data on the δ^{56}Fe of d-Fe in marine aerosol particles are limited due to analytical difficulties, including high filter blanks (Conway et al., 2019; Kurisu et al., 2021). Given that the fraction of anthropogenic Fe in d-Fe depends on the Fe_{sol}% of anthropogenic Fe and mineral dust, the contribution of anthropogenic Fe to the total Fe is not always directly reflected to that of d-Fe. Therefore, attaining the capability to produce indicators for source estimation of d-Fe in aerosol particles with low analytical difficulty is ideal.

The stoichiometry of the mineral dissolution of major elements (e.g., Si, Al, Fe, and Mg) has been investigated to understand the dissolution processes of minerals in the environment (Acker and Bricker, 1992; Brantley et al., 2008; Bibi et al., 2011; Bray et al., 2015). The stoichiometry of mineral dissolution is controlled by acid type, pH, and ionic strength and

the presence or absence of organic ligands (Brantley et al., 2008; Bray et al., 2015). Therefore, the ratios of dissolved concentrations of major elements vary depending on their dissolution processes from minerals (Acker and Bricker, 1992; Brantley et al., 2008; Bibi et al., 2011; Bray et al., 2015). However, studies on Fe dissolution from aerosols have focused exclusively on Fe and neglected other dissolved metals in aerosol particles. In general, although the stoichiometry of mineral dissolution is discussed based on the ratio of the dissolution rate of major elements versus that of Si (Acker and Bricker, 1992; Brantley et al., 2008; Bibi et al., 2011; Bray et al., 2015), the data on total and dissolved Si concentrations in aerosol particles are limited relative to those on Fe and Al concentrations (Jickells et al., 2016). Discussion of the dissolution processes of mineral dust using Mg concentration is difficult because Mg in marine aerosol particles is usually derived from sea spray aerosol. Therefore, this study focused on the molar ratio of d-Fe to dissolved Al ([d-Fe]/[d-Al]) as an indicator of the sources of d-Fe in aerosol particles because (i) previous studies have frequently determined d-Fe and d-Al concentrations in aerosol particles, and (ii) mineral dust is the dominant source of Fe and Al.

Iron-bearing particles derived from mineral dust and anthropogenic Fe have different chemical compositions and mineralogy. Mineral dust is mainly composed of crystalline aluminosilicates (Jeong and Achterberg, 2014; Jeong et al., 2014; Jeong, 2020). The fly ash emitted from anthropogenic high-temperature combustion processes can be categorized into two groups: non-magnetic and magnetic particles. Non-magnetic particles in fly ash consist of aluminosilicate glass (Furuya et al., 1987; Rivera et al., 2015). This fraction is dominated by poorly ordered polymerized hydroxyl Fe(III) (Rivera et al., 2015). The magnetic fraction is composed of crystalline Fe oxides (e.g., hematite and magnetite) formed through the condensation of evaporated Fe during gas cooling (Kukier et al., 2003; Fomenko et al., 2019; Czech, 2022). Magnetic and non-magnetic particles have been found in ambient aerosol particles (Li et al., 2021; Zhu, Y. et al., 2020, 2022). Therefore, differences in the mineralogy and chemical composition of mineral dust, magnetic, and non-magnetic particles possibly affect the [d-Fe]/[d-Al] ratio in aerosol particles. The [d-Fe]/[d-Al] ratio of clay minerals ranges from 0.100 to 1.00 (Kodama and Schnitzer, 1973; Lowson et al., 2005; Bibi et al., 2011; Bray et al., 2015), whereas that of fly ash emitted from coal and municipal solid-waste incinerators (MSWIs) is less than 0.100 (Seidel and Zimmels, 1998; Kim et al., 2003; Huang et al., 2007). In addition, the [d-Fe]/[d-Al] ratio of aggregates of Fe oxide nanoparticles derived from anthropogenic emissions is expected to be higher than that of mineral dust and fly ash because Fe oxide nanoparticles contain minimal amounts of coexisting elements (Kukier et al., 2003; Fomenko et al., 2019). If the [d-Fe]/[d-Al] ratio of mineral dust and anthropogenic Fe is generalized, the fractions of mineral dust and anthropogenic Fe in d-Fe in aerosol particles can be estimated based on the [d-Fe]/[d-Al] ratio.

In 2013, the annual observation of Fe, Al, and other trace metal concentrations and their fractional solubilities in size-fractionated aerosol particles (seven fractions) was conducted in Higashi-Hiroshima, Hiroshima, Japan (Fig. 1). Air masses at the sampling site in summer were mainly derived from the domestic region of Japan, whereas air masses passing over East Asia arrived at the site in winter and spring (Fig. S1). Our sample set included samples affected by Asian dust and serious haze events associated with anthropogenic emissions, which allowed us to obtain aerosol samples with considerable differences depending on the size dependence and seasonal variation expected for Fe chemistry and d-Fe sources. Ground-based long-term observations of Fe_{sol}% are important to complement the observed data on Fe_{sol}% in marine aerosols because (i) mineral

dust and anthropogenic Fe (excluding ship emissions) are emitted in continental regions, and (ii) the representativeness of Fe_{sol}% data obtained by ship-board observation is often problematic due to difficulties in the long-term observation of marine aerosol particles at fixed stations (Mahowald et al., 2018). In addition, mineral dust and anthropogenic Fe internally mixed with sulfate, nitrate, and organics are frequently found in the continental atmosphere, which indicates that chemical aging of Fe-bearing particles begins during transport in continental regions. Previous studies reported that atmospheric processing after passing over Japan has a small effect on the Fe_{sol}% of marine aerosol particles in the case of Fe-bearing particles during their transport from East Asia to the Pacific Ocean (Buck et al., 2013; Sakata et al., 2022). Japan is located at the rim of East Asia (or the entrance of the North Pacific Ocean), and thus, it can accumulate mineral dust and anthropogenic Fe aged during their transport from East Asia to Japan. Therefore, Japan can be an important observation site for the characterization of aerosols transported to North Pacific Ocean. This study aimed to evaluate the availability of source identification of d-Fe in aerosol particles based on [d-Fe]/[d-Al] ratios and gain insights into the seasonal variability of the fractions of mineral dust and anthropogenic Fe in d-Fe in aerosols.

2. Method

2.1. Aerosol sampling

Aerosol sampling was performed at Higashi-Hiroshima, Hiroshima, Japan (Fig. 1; 34.40°N, 132.71°E). Size-fractionated aerosol particles were collected using a high-volume air sampler (MODEL 123-SL, Kimoto, Japan) with a Sierra-type cascade impactor (TE-236, Tisch Environmental Inc., USA) installed on a roof 10 m above ground level. The cascade impactor had seven stages, and the aerodynamic diameters of the aerosol particles collected in each stage from Stage 1 to Stage 7 followed the order >10.2, 4.2–10.2, 2.1–4.2, 1.3–2.1, 0.69–1.3, 0.39–0.69, and <0.39 μm. The coarse aerosol particles were coarser than 1.3 μm (Stages 1–4), whereas the fine aerosol particles were finer than 1.3 μm (Stages 5–7). Aerosol particles were collected onto cellulose filters (Stages 1–6: TE-230WH, Tisch Environmental Inc., USA, and Stage 7: Whatman 41, 8 × 10 in^2, GE Healthcare, USA). Aerosol samplings during non-dust events were conducted every month from December 2012 to December 2013 (Table S1). The flow rate of the air sampler was fixed at 0.566 m^3 min^{-1}. The typical sampling period was 2 weeks. However, if the sampling flow rate decreased due to clogging of the Stage 7 filter, aerosol sampling was immediately stopped. Aerosol samplings were also performed during two dust events associated with haze and Asian dust on January 31, 2013 to February 1, 2013 and on March 4, 2013 to March 9, 2013, respectively. Aerosol mass concentrations in China exceeded 600 μg m^{-3} at the end of January 2013 (Tian et al., 2014; Wang et al., 2014), and their transported particles can be collected during the haze event. The sampling periods for the haze and Asian dust events were 1 and 5 days, respectively. The sampling periods for haze and Asian dust events were decided based on a chemical weather forecasting system, which predicted the mass concentrations of Asian dust and sulfate aerosols (Uno et al., 2004). Backward trajectories at the altitude of 100 m were calculated using the Hybrid Single-Particle Lagrangian-Integrated Trajectory model (Stein et al., 2015). Global Data

Assimilation System (GDAS 0.5 degree archive) was used to collect meteorological data. The total run time was 72 h, and the backward trajectory was calculated every 6 h. Figs. S1 and S2 show the backward trajectories for non-dust and dust events, respectively.

2.2. Major ion concentrations

Aerosol particles on approximately one-fourth of the filter strips were used for the extraction of major ions (Na^+, NH_4^+, K^+, Mg^{2+}, Ca^{2+}, Cl^-, NO_3^-, and SO_4^{2-}) using 5 mL ultrapure water (MQ, Merck Millipore, USA) in polypropylene vials with ultrasonication for 30 min. Suspended particles in the extract were removed using a hydrophilic polytetrafluoroethylene (PTFE) filter (ϕ: 0.20 μm, DISMIC, ADVANTEC, Tokyo Roshi Kaisha, Ltd., Japan). All materials used for the extraction of major ions were rinsed thrice with ultrapure water before use.

Major ion concentrations were determined through ion chromatography (ICS–1100, Dionex Japan, Japan). The guard columns for cations and anions were Dionex Ion Pack CG12A and AG22, respectively. The separation columns for cations and anions were Dionex CS12A and AS22, respectively. The eluents for cations and anions were methanesulfonic acids and a mixed solution of 4.5 mmol L^{-1} Na_2CO_3 and 1.4 mmol L^{-1} $NaHCO_3$, respectively. The detailed procedure of ion chromatography was described in the work of Sakata et al. (2014).

Non-sea-salt (nss) K^+, Mg^{2+}, Ca^{2+}, and SO_4^{2-} concentrations were estimated as follows:

$$[\text{nss-X}]_{\text{aerosol}} = [\text{Total-X}]_{\text{aerosol}} - [\text{Na}]_{\text{aerosol}} \times ([\text{X}]/[\text{Na}^+])_{\text{seawater}}, \text{ (Eq. 1)}$$

where X is the molar concentration of either K^+, Mg^{2+}, Ca^{2+}, or SO_4^{2-}. The molar ratios of $[K^+]/[Na^+]$, $[Mg^{2+}]/[Na^+]$, $[Ca^{2+}]/[Na^+]$, and $[SO_4^{2-}]/[Na^+]$ were 0.0213, 0.113, 0.0213, and 0.0596, respectively (Nozaki, 2001).

2.3. Estimation of aerosol pH

The aerosol pH of fine aerosol particles was estimated using the thermodynamic E-AIM Model IV (Clegg et al., 1998; Friese and Ebel, 2010). The calculation parameters for the model were $[H^+]$, $[NH_4^+]$, $[Na^+]$, $[Cl^-]$, $[NO_3^-]$, $[SO_4^{2-}]$, temperature, and relative humidity (RH). Ammonia gas concentration was not measured during the sampling campaign. Therefore, aerosol pH was calculated through a reverse mode that tended to overestimate aerosol acidity (Song and Osada, 2020). Previous studies have reported that nonvolatile cations (e.g., Mg^{2+} and Ca^{2+}) affect the calculation results of aerosol pH (Guo et al., 2018; Pye et al., 2020). $[Na^+]$ was used as a representative of nonvolatile cations (= $[Na^+] + [K^+] + 2 \times [Mg^{2+}] + 2 \times [Ca^{2+}]$) to estimate aerosol pH because the E-AIM model IV cannot incorporate the concentrations of nonvolatile cations other than Na^+ (Tao and Murphy, 2019a). The $[H^+]$ concentration in aerosol particles was estimated on the basis of charge balance. Several samples had negative $[H^+]$ concentrations and were thus excluded from the estimation of aerosol pH. In addition, E-AIM model IV cannot calculate aerosol pH when the RH is below 60 %. The average RH during each sampling period was higher than 60 %, except for those of aerosol samples collected in April and May 2013. The aerosol pH collected in April and May was calculated under the assumption of 60 % RH because the average RHs of the samples for these months were 59.4 % and 59.5 %, respectively. Aerosol pH was calculated using the following equation:

$$\text{Aerosol pH} = -\log_{10}(m_{H+} \times \gamma_{H+}), \text{ (Eq. 2)}$$

where m_{H+} and γ_{H+} are the molar fraction and activity coefficient of H^+, respectively.

175

2.4. Trace metal concentrations

Approximately one-fourth of the filter strips were used for acid digestion to determine the total trace metal concentrations. Each filter piece was digested with a mixed acid solution of 15.2 mol L^{-1} HNO_3, 9.3 mol L^{-1} HCl, and 20 mol L^{-1} HF in a 7 mL perfluoroalkoxyalkane vial heated at 120 °C for 12 h (all mineral acids were procured from TAMAPURE AA-100, Tama
180 Chemicals Co., Ltd., Japan). Subsequently, the mixed acid was evaporated to dryness. The dried residue was dissolved in 5 mL 0.15 mol L^{-1} HNO_3 heated at 120 °C for 3 h. The solution was filtered through a hydrophilic PTFE filter (ϕ: 0.20 μm, Dismic®, 25HP020AN, Advantec, Japan) to prepare the analytical solution. Soluble metals in aerosol particles were extracted using 5 mL ultrapure water with ultrasonication for 30 min. Then, the extracted solution was filtrated with a hydrophilic syringe PTFE filter. The filtrated solution was acidified to prepare a 0.15 mol L^{-1} HNO_3 solution by the addition of 15.3 mol L^{-1} HNO_3.
185 The filtrated solutions for total and dissolved metal concentration analyses were diluted with 0.15 mol L^{-1} HNO_3 by factors of 10–1000.

The total and dissolved metal concentrations of the sample solution were determined via inductively coupled plasma mass spectrometry (ICP–MS, Agilent 7700, Agilent, Japan). The sample introduction system consisted of a borosilicate nebulizer (MicroMist, Agilent, Japan) and a quartz Scott double-pass spray chamber. The elements in the sample solution were
190 ionized by argon plasma (RF power: 1500 W, Ar flow for career gas: 1.0 L min^{-1}). The ions were introduced into the detection system by passing them through nickel sampling and skimmer corns. The ion beam was focused with x-type ion lenses. Helium collision mode was used to reduce interference from oxides (e.g., $^{40}Ar^{16}O+$ for ^{56}Fe). Helium gas was injected into a dynamic reaction cell at a rate of 3.6 mL min^{-1}. Then, mass selection was performed on a quadrupole system. Target metal concentrations were measured in pulse (ion-counting) mode. The sensitivity drift during measurements was corrected using the internal
195 standard of 1 ng g^{-1} indium.

2.5. Estimation of EF of Fe and Fe_{sol}%

The total and dissolved metal concentrations in TSP were calculated by the summation of the target metal concentrations in all sampling stages. Crustal and non-crustal Fe concentrations and the EF of target metals normalized by the average
200 continental crust were calculated by using the following equations:

$$\text{Crustal Fe} = Al_{crust} \times (Fe/Al)_{aerosol}, \text{ (Eq. 3)}$$

$$\text{Non-crustal Fe} = \text{Total Fe} - \text{crustal Fe}, \text{ (Eq. 4)}$$

$$EF = (M/Al)_{aerosol}/(M/Al)_{crust}, \text{ (Eq. 5)}$$

where M is the target metal. Iron and Al concentrations in the average continental crust (Fe/Al: 0.684) were acquired by
205 referring to Taylor (1964). Given the variability of the Fe/Al ratio in crustal materials, significant enrichment of the Fe derived

from anthropogenic emissions is usually recognized at EF values higher than 10.0. The EF equation suggests that about 90 % of Fe is derived from anthropogenic sources when the EF is 10.0. Given that the emission amount of crustal Fe is an order of magnitude higher than that of anthropogenic Fe, the EF for Fe in aerosol particles is usually below 10.0, except for aerosol samples collected near steel plants and in urban areas. Therefore, classification of Fe as anthropogenic Fe by the criterion EF > 10.0 substantially simplifies the origin of Fe in aerosol particles. If the variation of Fe/Al ratio in natural-source aerosol is limited in a narrow range, aerosols with EF > 2.00 can still be evaluated as aerosol samples containing anthropogenic Fe component to a certain degree. The small variability of the Fe/Al ratio in desert soil in East Asia was confirmed (average ± 1σ standard deviation (ave.±1σ): 0.555 ± 0.170, range: 0.294–1.05, Nishikawa et al., 2013; Ding et al., 2001; Cao et al., 2008; Liu, X. et al., 2022 and references therein). The Fe/Al ratio in mineral dust exhibits a small variability, and thus, enrichment of anthropogenic Fe is recognized when the EF of Fe is higher than 2.00 (Fe/Al > 1.37). The Fe_{sol}% in aerosol samples was calculated by using the following equation:

Fractional solubility (%) = (d-Fe/total M) × 100. (Eq. 6)

3. Results and Discussion

3.1. Total Fe and Al concentrations

The total Fe and Al concentrations in the TSP collected during the non-dust event were 256–1561 and 170–1716 ng m^{-3}, respectively (Figs. 2a and 2b). Coarse aerosol particles accounted for 69.4 ± 7.2 % and 72.9 ± 7.6 % of the total Fe and Al in TSP, respectively. The total Fe and Al concentrations were higher in spring (March to May) and Asian dust events than in other seasons (Figs. 2a and 2b). A higher Ca^{2+} concentration, as a marker of Asian dust, was also observed in spring than in other seasons (Fig. S3b, Supplemental Note). Therefore, the high Fe and Al concentrations in spring were due to the strong influence of Asian dust (Figs. 2a and 2b). The average EF of Fe in the TSP samples collected from summer to fall (June to October) was 2.84 ± 0.83 when air masses mainly originated from Japan (Fig. S6a). By contrast, the average EF of Fe in the TSP derived from East Asia in winter and spring was 1.57 ± 0.35 (Fig. S6a). Thus, the influences of anthropogenic emission on the total Fe in TSP are more significant in the air mass derived from Japan than that from East Asia (Figs. S1, S2, and S6a). The total Al concentrations sharply decreased from May to June, whereas the decrease in the total Fe concentrations was not as significant (Figs. 2a and 2b). This result indicated that the aerosol particles emitted in Japan contained non-crustal Fe. In addition, the total Fe concentration in the haze event was almost the same as that in the Asian dust event, whereas the total Al concentration in the haze event was lower than that in the Asian dust event. This result demonstrated that during haze events, the total Fe concentrations were significantly enhanced by the non-crustal Fe emitted from anthropogenic emissions.

The average EFs of Fe in coarse and fine aerosol particles were 1.99 ± 0.89 and 2.49 ± 1.09, respectively (Figs. 2c and S6a). Therefore, non-crustal Fe may be present in coarse and fine aerosol particles. Non-crustal Fe concentration in coarse aerosol particles correlated with Cu, Zn, and Sb (r > 0.500, Table S2). These elements in coarse aerosol particles are known as

tracer elements of fragment vehicle-related materials in road dust (brake dust: Cu and Sb, and tire wear: Zn) (Adachi and Tainosho, 2004; Wåhlin et al., 2006; Iijima et al., 2007; Gietl et al., 2010; Harrison et al., 2021). The correlation coefficient of non-crustal Fe with Cu as a tracer element of brake pads was the highest among these tracer elements (r: 0.747, Table S2). Fe is the most dominant metal in brake rings (up to 50 wt%), and its concentration is about an order of magnitude higher than that of Al in brake pads. Therefore, brake pads can increase the EF of Fe in aerosol particles. The EF of Fe in road dust (<40 μm) collected from tunnels and roadsides around the sampling site were 3.41 and 6.04, respectively. Therefore, resuspensions of brake pad fragments in road dust can be considered non-crustal Fe in coarse aerosol particles. This result is consistent with the finding of a previous model study, which showed that road dust was the dominant source of Cu and non-crustal Fe in PM_{10} in the Chugoku–Shikoku area (the locality around the sampling site) (Kajino et al., 2020).

In fine aerosol particles, non-crustal Fe concentrations were correlated with Zn, Sb, Cd, and Pb emitted from high-temperature combustions, including coal combustion, MSWI, and steel/iron industrial processes (r > 0.700, Table S3, Pacyna and Pacyna, 2001; Sakata et al., 2000; Sakata et al., 2014; Kajino et al., 2020). These high-temperature combustion processes emit nanoparticles of hematite and magnetite, which can increase the EF of Fe in fine aerosol particles. The negative δ^{56}Fe associated with hematite derived from high-temperature combustion processes was detected in aerosol samples collected at the same sampling site (Kurisu et al., 2016a). Therefore, the nanoparticles of hematite and magnetite are likely the dominant sources of non-crustal Fe in fine aerosol particles. In addition, in fine aerosol particles, the non-crustal Fe concentration correlated with V as a tracer element of heavy-oil combustion (Nriagu and Pacyna, 1988); however, the correlation factor between non-crustal Fe and V was lower than those of Zn, Sb, Cd, and Pb (r: 0.601, Table S3). A previous model study predicted that V around the sampling site was derived from vessel emissions in the Seto Inland Sea (Kajino et al., 2020), which is located at the southern part of the sampling site (Fig. 1). Our results also showed that V concentrations in fine aerosol particles were higher from July to September, during which air masses passed through the Seto Inland Sea than in other periods (Figs. 1 and S7a). At this point, the concentrations of Zn, Sb, and Pb did not increase (Figs. S7b–S7d). Therefore, in addition to the high-temperature combustion processes mentioned above, heavy-oil combustion processes around the Seto Inland Sea were possible emission sources of the non-crustal Fe in fine aerosol particles collected in summer.

3.2. Size distributions of d-Fe and d-Al concentration and their fractional solubility

The concentrations of d-Fe and Al in the TSP collected during the non-dust event ranged from 11.4 ng m^{-3} to 65.0 ng m^{-3} and from 8.30 ng m^{-3} to 40.6 ng m^{-3}, respectively (Figs. 3a and 3d). The Fe_{sol}% and Al_{sol}% of the TSP ranged from 2.00 % to 7.73 % and 1.46 % to 7.39 %, respectively (Figs. S6b and S6c), which were within the typical range of Fe_{sol}% in the TSP collected from East Asia and north-western Pacific Ocean (Buck et al., 2006, 2013; Takahashi et al., 2013; Sakata et al., 2022). Although approximately 70 % of the total Fe and Al in the TSP were present in coarse aerosol particles, high concentrations of d-Fe and d-Al were found in fine aerosol particles (Figs. 3a and 3d). The average d-Fe and d-Al concentrations of fine aerosol particles were 27.3 ± 17.4 and 14.3 ± 10.9 ng m^{-3}, which accounted for 72.0 ± 8.9 % and 53.1 ± 9.9 % of d-Fe and d-Al in the TSP, respectively. Enrichment of d-Fe and d-Al in fine aerosol particles has been reported not only in the urban

atmosphere (Fang et al., 2017; Hsieh et al., 2022; Liu, L. et al., 2022) but also in the marine atmosphere (McDaniel et al., 2019; Baker et al., 2020; Sakata et al., 2022). These previous studies have reported that the higher amounts of d-Fe and d-Al in fine aerosol particles than coarse aerosol particles were caused by either or both (i) contamination of the anthropogenic aerosol with high Fe_{sol}% and Al_{sol}% and (ii) solubilization of Fe and Al in fine aerosol particles by atmospheric processes. The average Fe_{sol}% in fine aerosol particles in this study (11.4 ± 7.0 %) was about five times higher than that of coarse aerosol particles (2.19 ± 2.27 %, Figs. 3b and 3c). In the case of Al, fine aerosol particles (8.82 ± 6.48 %) yielded about twice as much as the Al_{sol}% of coarse aerosol particles (3.25 ± 3.41 %, Figs. 3e and 3f). These results indicated that the Fe in fine aerosol particles is more susceptible to dissolution in water by anthropogenic activities and chemical aging than Al. The Fe_{sol}% and Al_{sol}% in coarse aerosol particles were higher than those in desert dust soil (typical Fe_{sol}% and Al_{sol}%: 0.100 %). Therefore, the Fe_{sol}% and Al_{sol}% in coarse aerosol particles increased due to anthropogenic aerosol and/or atmospheric processes, but the effect was not as pronounced as in fine aerosol particles.

3.3. Possible factor controlling Fe_{sol}% and Al_{sol}%

3.3.1. Coarse aerosol particles

Non-crustal Fe in coarse aerosol particles was derived from brake pads and tire ware debris in road dust as mentioned above. If road dust is the dominant source of d-Fe in coarse aerosol particles, then the d-Fe concentration correlates with non-crustal Fe concentration. However, no correlation was found between non-crustal Fe and d-Fe concentrations in coarse aerosol particles (r: 0.352). Thus, road dust was not the source of d-Fe in coarse aerosol particles. This result is consistent with that of previous studies in which the Fe_{sol}% of brake pads and tire wear debris was lower than 0.01 % (Shupert et al., 2013; Halle et al., 2021).

The Fe_{sol}% and Al_{sol}% of coarse aerosol particles increased with the decrease in aerosol diameter (Figs. 3b, 3c, 3e, and 3f). Specific surface area is one of the factors controlling Fe_{sol}% and Al_{sol}% in aerosol particles (Baker and Jickells, 2006, 2017; McDaniel et al., 2019), and the chemical reactivity of aerosol particles increases with the increase specific surface area (decrease in aerosol diameter). Previous studies have reported that chemical aging of coarse aerosol particles by acidic species, including HNO_3 and H_2SO_4, solubilized Fe in aerosol particles (Takahashi et al., 2011; Zhu et al., 2022). The Fe_{sol}% and Al_{sol}% of coarse aerosol particles correlated with the molar concentration ratios of nns-SO_4^{2-} relative to the total Al or total Fe (Fig. 4a), [nss-SO_4^{2-}]/[total Fe], and [nss-SO_4^{2-}]/[total Al]). This result is consistent with previous findings showing that aluminosilicates in aerosol particles react preferentially with H_2SO_4 (Sullivan et al., 2007; Fitzgerald et al., 2015). Furthermore, our previous studies showed that the relative abundance of ferrihydrite formed by hydrolysis of Fe in coarse aerosol particles increased with the decrease in diameter (Takahashi et al., 2011; Sakata et al., 2022). These results indicate that atmospheric processes of coarse aerosol particles by H_2SO_4 promoted the formation of d-Fe via proton-promoted dissolution or hydrolysis of Fe. By contrast, no good correlation of Fe_{sol}% and Al_{sol}% with [NO_3^-]/[total Fe] and [NO_3^-]/[total Al] was found because HNO_3 reacts mainly with Ca-rich particles (e.g., $CaCO_3$) in mineral dust (Fig. 4b, Karydis et al., 2016; Kakavas et al., 2021).

3.3.2. Fine aerosol particles

Unlike the d-Fe in coarse aerosol particles, the d-Fe concentrations in fine aerosol particles correlated with non-crustal Fe concentrations (Fig. 5a). Good correlations of d-Fe in fine aerosol particles with concentrations of V, Zn, Sb, and Pb as tracer elements for high-temperature combustions were also found (Figs. 5b–5e). The correlation coefficient between d-Fe and Zn was the largest (Fig. 5c). Zinc in fine aerosol particles from the sampling sites originated from various high-temperature combustions, including those in MSWIs, steel/iron industries, and coal power plants (Kajino et al., 2020). Therefore, the non-crustal Fe emitted from high-temperature combustion is one of the dominant sources of d-Fe in fine aerosol particles although identification of specific sources of non-crustal d-Fe around the sampling site was difficult. This result is consistent with our previous study, which showed that negative δ^{56}Fe associated with high-temperature combustions was detected in fine aerosol particles (Kurisu et al., 2016a).

In addition to the input of non-crustal Fe with high Fe_{sol}% in fine aerosol particles, aerosol acidification resulted in the high Fe_{sol}% and Al_{sol}% in fine aerosol particles (Fang et al., 2017; Sakata et al., 2022). Along with coarse aerosol particles, Fe_{sol}% and Al_{sol}% in fine aerosol particles did not correlate with [NO_3^-]/[total Fe] and [NO_3^-]/[total Al] due to the preferential reaction of HNO_3 with Ca^{2+} (Fig. 4d). The Fe_{sol}% and Al_{sol}% correlated with [nss-SO_4^{2-}]/[total Fe] and [nss-SO_4^{2-}]/[total Al], respectively (Fig. 4c). Moreover, these solubilities increased with the decrease in aerosol pH (Fig. 4e), which indicates that acidification of fine aerosol particles by H_2SO_4 plays a significant role in Fe solubilization. These results are reasonable and supported by previous studies reporting that mineral dust and anthropogenic Fe in fine aerosol particles were covered by sulfate, and internal mixing of these particles with sulfate promoted the dissolution of Fe (Sullivan et al., 2007; Fitzgerald et al., 2015; Li et al., 2017, Zhu, Y. et al., 2020, 2022). However, compared with the correlation factor of Fe_{sol}% with [nss-SO_4^{2-}]/[total Fe], coarse aerosol particles yielded a higher correlation factor than fine aerosol particles (Figs. 4a and 4c). Similar results have been reported by previous studies on Fe_{sol}% in China, which indicated the presence of anthropogenic Fe with high Fe_{sol}% as one of the reasons for the low value of the correlation factor (Zhang et al., 2022, 2023). Therefore, the low correlation between Fe_{sol}% and [nss-SO_4^{2-}]/[total Fe] of fine aerosol particles implied that acidification of mineral dust was not the sole factor controlling Fe_{sol}%.

4. Establishment of source estimation method for d-Fe using the [d-Fe]/[d-Al] ratio

4.1. [d-Fe]/[d-Al] ratio in coarse aerosol particles and mineral dust

Correlation analysis between non-crustal Fe and d-Fe concentrations revealed that non-crustal Fe contributed to the source of d-Fe in fine aerosol particles but not in coarse aerosol particles. Correlation analysis is a simple method used to evaluate emission sources of d-Fe in aerosol particles. However, quantitative estimations of the fraction of non-crustal Fe to d-Fe in aerosol particles present a challenge. Therefore, a quantitative indicator is preferable for the assessment of the relative abundance of non-crustal Fe to d-Fe. This study investigated the evaluation of the fraction of non-crustal Fe to d-Fe using the [d-Fe]/[d-Al] ratio. One of the reasons is that the [d-Fe]/[d-Al] ratio in mineral dust differs from that in non-crustal sources, as will be discussed below (Fig. 6a). In addition, the [d-Fe]/[d-Al] ratio may vary depending on the extraction method and aging

process of aerosol particles (Fig. 6a, e.g., proton-promoted versus ligand-promoted dissolutions). The [d-Fe]/[d-Al] ratio in fine aerosol particles (ave.±1σ: 1.15 ± 0.80) differed from that in coarse aerosol particles (Fig. 6b, ave.±1σ: 0.408 ± 0.168). With the evaluation of the fraction of non-crustal Fe to d-Fe in aerosol particles, the [d-Fe]/[d-Al] ratios of crustal and non-crustal Fe can be generalized.

Biotite, illite, and Fe-rich chlorite are considered representative mineral species of aluminosilicates in aerosol particles because they are detected in aerosol particles collected in East Asia (Takahashi et al., 2011; Kurisu et al., 2016a; Sakata et al., 2022). When Fe and Al in these aluminosilicates were dissolved by proton-promoted dissolution (pH 1.0–7.0) under oxic conditions, the [d-Fe]/[d-Al] ratios of biotite, illite, and Fe-rich chlorite were within 0.427–0.930 (ave.±1σ: 0.776 ± 0.152), 0.156–0.689 (ave.±1σ: 0.404 ± 0.189), and 0.142–1.03 (ave.±1σ: 0.699 ± 0.303), respectively (Fig. 6a; Kodama and Schnitzer, 1973; Lowson et al., 2005; Bibi et al., 2015; Bray et al., 2015). In addition, the average [d-Fe]/[d-Al] ratios of Asian dust, Saharan dust, and Arizona test dusts obtained by proton-promoted dissolution were 0.238 ± 0.201, 0.163 ± 0.157, and 0.230 ± 0.009, respectively (Fig. 6a, Desboeufs et al., 2001; Duvall et al., 2008; Shi et al., 2011). The [d-Fe]/[d-Al] ratio decreased with the increase in pH due to either or both the preferential retention of Fe in the mineral phase and precipitation of secondary ferrihydrite under near-neutral conditions (Fig. S8, Kodama and Schnitzer, 1973; Desboeufs et al., 2001; Lowson et al., 2005; Bray et al., 2015). Thus, the [d-Fe]/[d-Al] ratio obtained from the proton-promoted dissolution of the mineral dust was between 0.100 and 1.00.

Organic ligands promote the dissolution of Fe from the mineral phase through the direct complexation of organic ligands with Fe at the mineral surface and reduction of the saturation index of inorganic Fe in aqueous phase due to the formation of organic complexes of Fe (Chen and Grassian, 2013; Paris and Desboefus, 2013; Wang et al., 2017). The [d-Fe]/[d-Al] ratios of biotite and Fe-rich chlorite associated with ligand-promoted dissolution were 0.795–3.83 (ave.±1σ: 1.20 ± 0.66) and 1.19–1.37 (ave.±1σ: 1.31 ± 0.06), respectively (Kodama and Schnitzer, 1973; Bray et al., 2015). A previous study showed that the [d-Fe]/[d-Al] ratios of coarse aerosol particles extracted by 20 mmol L^{-1} oxalate at pH 4.7 (1.31 ± 0.42) were higher than that of ultrapure water extraction (0.354 ± 0.714) (*Coarse aerosol (Proton) and Coarse aerosol (Ligand)* in Fig. 6a, Kurisu et al., 2019). Thus, the [d-Fe]/[d-Al] ratio associated with ligand-promoted dissolution was higher than that associated with proton-promoted dissolution (Fig. 6a). The higher stability constant (log *K*) of Fe^{3+} than that of Al^{3+} with organic ligands (e.g., log *K* of $AlC_2O_4^+$: 7.73, log *K* of $FeC_2O_4^+$: 9.15) caused the preferential dissolution of Fe over Al from mineral dust, which increased the [d-Fe]/[d-Al] ratio.

The [d-Fe]/[d-Al] ratio of coarse aerosol particles collected by this study (n = 60, average: 0.121–0.927) was within the range of [d-Fe]/[d-Al] ratios of mineral dust that underwent proton-promoted dissolutions, and it increased with the increase in Fe_{sol}% (Fig. 6b, r: 0.552). As previously mentioned, [d-Fe]/[d-Al] and Fe_{sol}% obtained by proton-promoted dissolution of mineral dust increased with the decrease in pH, which is consistent with the correlation between Fe_{sol}% and [nss-SO_4^{2-}]/[total Fe] in coarse aerosol particles (Fig. 4a). Therefore, the proton-promoted dissolution of mineral dust is the dominant source of d-Fe in coarse aerosol particles. By contrast, no coarse aerosol particles had [d-Fe]/[d-Al] ratios higher than 1.0 (Fig. 6b),

which indicates that the effect of organic ligands on the solubilization of Fe and Al in coarse aerosol particles was insignificant. In addition, the non-crustal Fe derived from road dust was not a factor controlling the [d-Fe]/[d-Al] ratio in coarse aerosol particles due to the lack of correlation between the [d-Fe]/[d-Al] ratio and EF of Fe. This result is reasonable because the Fe_{sol}% of brake pads and tire wear debris was less than 0.01 % (Shupert et al., 2013; Halle et al., 2021).

4.2. [d-Fe]/[d-Al] ratio in fine aerosol particles and their emissions

The average [d-Fe]/[d-Al] ratio of fine aerosol particles (n = 45, ave.±1σ: 1.15 ± 0.80, range: 0.386–4.67) was higher than those of coarse aerosol particles and mineral dust (Figs. 6a and 6b). The [d-Fe]/[d-Al] ratios of several fine aerosol particles exceeded 1.5, which was beyond the range of the ratio of mineral dust that underwent ligand-promoted dissolutions (Fig. 6a and 6b). Given the good correlation between the [d-Fe]/[d-Al] ratio and EF of Fe (r: 0.505), the [d-Fe]/[d-Al] ratio higher than 1.5 was attributed to non-crustal Fe (Fig. 6c). The non-crustal Fe in fine aerosol particles was derived from fly ash produced by high-temperature combustions, including steel/iron industrial processes, MSWI, and coal and fuel oil combustion. Fly ash contains two types of particles, namely, magnetic and non-magnetic particles (Kukier et al., 2003; Fomenko et al., 2021). Given the different elemental compositions and Fe species of between magnetic and non-magnetic particles, the influences of these particles on the [d-Fe]/[d-Al] ratio and Fe_{sol}% in fine aerosol particles were evaluated separately

4.2.1. [d-Fe]/[d-Al] ratio of non-crustal Fe: magnetic particles

The mass fraction of magnetic particles accounts for a small percentage of the total fly ash mass (Hansen et al., 1981), but up to 90 % Fe in fly ash was present as magnetic particles (Kukier et al., 2003). Iron species of magnetic particles in fly ash are mainly composed of Fe oxides, including hematite and magnetite. The iron concentration in magnetic particles reaches up to 60 %–70 %, whereas that of Al typically amounts to up to 10 % (Kukier et al., 2003; Fomenko et al., 2021). This result indicated that Fe in magnetic particles in fly ash can increase the EF of fine aerosol particles.

Previous studies have reported that d-Fe in fine aerosol particles yielded negative $\delta^{56}Fe$ (Kurisu et al., 2016a, 2019), and recent research showed negative $\delta^{56}Fe$ in magnetic particles in $PM_{2.5}$ (Zuo et al., 2021). The magnetic particles in fine fractions (<1.0 μm) are considered formed by either or both the fragmentation of large particles and condensation of vaporized Fe. The Fe-oxides formed by condensation of vaporized Fe (hereafter high-temp-FeOx) is one of the important sources of d-Fe in fine aerosol particles because the high-temp-FeOx yield negative $\delta^{56}Fe$, which is formed by kinetic Fe isotope fractionation during vaporization (Kurisu et al., 2016a, 2019). The high-temp-FeOx can increase the [d-Fe]/[d-Al] ratio of fine aerosol particles because the [d-Fe]/[d-Al] ratio of fine aerosol particles with low $\delta^{56}Fe$ (<–1.0‰) collected near a steel plant was higher than 1.5 when extracted with proton- (ultrapure water) and ligand-promoted (20 mmol/L oxalic acid at pH 4.7) dissolutions (*Anthropogenic Fe in fine aerosols (Proton) and Anthropogenic Fe in fine aerosols (Ligand)* in Fig. 6a; Kurisu et al., 2019). However, the Fe_{sol}% in magnetic particles in coal fly ash was less than 0.100 % in weakly acidic solutions (Kukier et al., 2003), which was considerably lower than the Fe_{sol}% in fine aerosol particles (11.4 ± 7.0 %). As previously mentioned, the Fe_{sol}% in

fine aerosol particles increased with the increase in [nss-SO_4^{2-}]/[total Fe] and with the decrease in aerosol pH (Figs. 4c and 4e, respectively). In addition, at a high Fe_{sol}% (>10 %), the aerosol pH was lower than 3.0, which was consistent with previous observations (Tao and Murphy, 2019b). Therefore, aerosol acidification is also a dominant factor that controls Fe_{sol}% in fine aerosol particles.

As for fine aerosol particles with [d-Fe]/[d-Al] between 1.00 and 1.50, the effect of ligand-promoted dissolution of mineral particles should be considered (Fig. 6b). If ligand-promoted dissolution of mineral dust is the dominant source of d-Fe in fine aerosol particles, the correlation between the [d-Fe]/[d-Al] ratio and EF of Fe should not be observed because the EF of mineral dust should be about 1.00. Therefore, the high [d-Fe]/[d-Al] ratio in fine aerosol particles was attributed to the presence of high-temp-FeOx rather than ligand-promoted dissolution of mineral dust.

4.2.2. [d-Fe]/[d-Al] ratio of non-crustal Fe: non-magnetic fraction of fly ash

Non-magnetic particles are mainly composed of amorphous aluminosilicate glasses, which are formed by the melting of crystalline aluminosilicate or chemical reactions of melted Al_2O_3 and SiO_2 (Zhang et al., 2007). Although previous studies did not perform the separation of magnetic and non-magnetic particles, the average [d-Fe]/[d-Al] ratio of coal and MSWI fly ash under acidic and circumneutral conditions was 0.104 ± 0.075 (Fig. 6a, Seidel and Zimmels, 1998; Praharaj et al., 2002; Kim et al., 2003; Huang et al., 2007; Chang et al., 2009; Gitari et al., 2009; Komonweeraket et al., 2015). Given the high [d-Fe]/[d-Al] ratio in the magnetic particles mentioned above, the [d-Fe]/[d-Al] ratio of non-magnetic particles should be less than 0.1 (Fig. 6a). Such a low [d-Fe]/[d-Al] ratio has not been detected in fine aerosol particles, which indicates that non-magnetic aluminosilicate glass in fly ash is not a dominant source of d-Fe (Fig. 6b). Furthermore, the EF of Fe in non-magnetic aluminosilicate glass emitted from MSWI and coal fly ash is almost 1, which cannot explain the correlation between EF and Fe_{sol}% for these particles (Sakata et al., 2022; Li et al., 2022). Therefore, the non-magnetic aluminosilicate glass derived from coal combustion and MSWI is possibly not a dominant source of aerosol particles with high Fe_{sol}% and [d-Fe]/[d-Al] ratio in fine aerosol particles.

In the case of heavy-oil combustion, Fe_{sol}% in oil fly ash can reach 80 % under circumneutral pH conditions due to the presence of water-soluble Fe(III)-sulfate (Schroth et al., 2009; Oakes et al., 2012). In addition, the fly ash emitted from heavy-oil combustions may be a source of d-Fe in fine aerosol particles collected in summer. Despite the limited data, the [d-Fe]/[d-Al] ratios of oil fly ash reached 0.403, 1.07, and 7.00 at pH 5.7, 4.7, and −0.3, respectively (Akita et al., 1995; Desboeufs et al., 2001). With the assumption of a linear relationship between the dissolution pH and [d-Fe]/[d-Al] ratio of heavy-oil fly ash, the expected [d-Fe]/[d-Al] ratio of heavy-oil ash was approximately 4.0 at the average aerosol pH in fine aerosol particles collected in summer (average: 2.11 ± 0.45). However, heavy oil fly ash was not the source of fine aerosol particles with high EF of Fe and [d-Fe]/[d-Al] ratio because the EF of Fe in heavy-oil fly ash was almost 1.0 as well as non-magnetic aluminosilicates of coal and MSWI (Sakata et al., 2017).

4.3. Fractions of crustal Fe and high-temp-FeOx in d-Fe and their Fe_{sol}%

4.3.1. Estimation method for the fractions of crustal and high-temp-FeOx and their Fe_{sol}%

The fractions of d-Fe derived from crustal Fe and high-temp-FeOx in d-Fe in fine aerosol particles were estimated based on the [d-Fe]/[d-Al] ratio. Hereafter, the fractions of d-Fe derived from crustal Fe and high-temp-FeOx are denoted as F_{crust} and F_{anthro}, respectively. In consideration of the binary mixing of d-Fe derived from mineral dust and high-temp-FeOx, the F_{anthro} in fine aerosol particles and F_{anthro} in TSP ($F_{anthro\text{-}TSP}$) were estimated with the following equations:

$$F_{crust} + F_{anthro} = 1, \text{ (Eq. 7)}$$

$$[\text{d-Fe}]/[\text{d-Al}]_{aerosol} = ([\text{d-Fe}]/[\text{d-Al}])_{crust} \times F_{crust} + ([\text{d-Fe}]/[\text{d-Al}])_{anthro} \times F_{anthro}, \text{ (Eq. 8)}$$

where $([\text{d-Fe}]/[\text{d-Al}])_{aerosol}$ is the [d-Fe]/[d-Al] ratio in aerosol particles. The $([\text{d-Fe}]/[\text{d-Al}])_{crust}$ and $([\text{d-Fe}]/[\text{d-Al}])_{anthro}$ are the representative values of [d-Fe]/[d-Al] ratios of mineral dust and anthropogenic Fe, respectively. Here, the $([\text{d-Fe}]/[\text{d-Al}])_{crust}$ and $([\text{d-Fe}]/[\text{d-Al}])_{anthro}$ were defined based on our observational results. The average [d-Fe]/[d-Al] ratio in coarse aerosol particles (0.408) was used as a representative $([\text{d-Fe}]/[\text{d-Al}])_{crust}$, and its value was within the range of proton-promoted dissolution of mineral dust (Figs. 6a and 6b). Given that the $([\text{d-Fe}]/[\text{d-Al}])_{anthro}$ has not been reported by previous studies, its two types were used in the calculation. The $([\text{d-Fe}]/[\text{d-Al}])_{anthro}$ was 4.67, which was the highest value observed in fine aerosol particles. Another $([\text{d-Fe}]/[\text{d-Al}])_{anthro}$ was the average [d-Fe]/[d-Al] ratio of fine aerosol particles with [d-Fe]/[d-Al] ratios higher than 1.5. At this time, the $([\text{d-Fe}]/[\text{d-Al}])_{anthro}$ was 2.08. When the average [d-Fe]/[d-Al] was used for the calculation, the F_{anthro} was higher than the value calculated by the highest$([\text{d-Fe}]/[\text{d-Al}]_{)anthro}$ (Figs. S9a and S9b). F_{anthro} was calculated using the average $([\text{d-Fe}]/[\text{d-Al}])_{anthro}$ to avoid underestimation.

Finally, the Fe_{sol}% of crustal and high-temp-FeOx (crustal-Fe_{sol}% and anthro-Fe_{sol}%) in fine aerosol particles were estimated through the following equations:

$$\text{Crustal-}Fe_{sol}\% = [(\text{d-Fe} \times F_{crustal})/\text{crustal Fe}] \times 100, \text{ (Eq. 9)}$$

$$\text{Anthro-}Fe_{sol}\% = [(\text{d-Fe} \times F_{anthro})/\text{non-crustal Fe}] \times 100. \text{ (Eq. 10)}$$

Crustal and non-crustal Fe concentrations were calculated using Eqs. 3 and 4, respectively.

4.3.2. Size dependence and seasonal variation of F_{anthro}

The annual average $F_{anthro\text{-}TSP}$ was 19.9 ± 19.2 % (Fig. 7a, range: 1.48–80.7 %). The $F_{anthro\text{-}TSP}$ was higher in summer–fall with the influence of Japanese air mass (average: 29.4 ± 25.8 %, range: 9.41–80.7 %) than in winter–spring with the influence of Asian outflow (Fig. 7a, average: 13.5 ± 10.6 %, range: 1.48–34.4 %). The high $F_{anthro\text{-}TSP}$ in summer was attributed to the high EF of Fe and [d-Fe]/[d-Al] ratio in the season. From the viewpoint of size dependence of F_{anthro}, the largest F_{anthro} in summer–fall and winter–spring was found in the finest and 0.39–0.69 μm fractions, respectively (Fig. 7b). These results are consistent with the source apportionment of Fe using δ^{56}Fe at the same sampling site because (i) the contribution of anthropogenic Fe to d-Fe in fine aerosol particles was more significant in summer than in spring due to the low δ^{56}Fe, and (ii) the lowest δ^{56}Fe was found in the finest and 0.39–0.69 μm fractions in summer and spring, respectively. Thus, the source estimation of Fe using [d-Fe]/[d-Al] is consistent with that which uses δ^{56}Fe.

Given the Fe supply to the Pacific Ocean, spring is the most important season throughout the year because approximately half of aerosol transport events from East Asia to the Pacific Ocean occurred in spring between 2007 and 2016, and they were mainly associated with mineral dust events (Zhu, Q., 2020). In addition, atmospheric Fe is supplied to the surface ocean by an episodic dust event that accounts for approximately 30 %–90 % of annual Fe depositions within 5 % of the days in a year (Mahowald et al., 2009). In consideration of these facts with the estimation results of $F_{\text{anthro-TSP}}$ and $F_{\text{crust-TSP}}$, mineral dust was the dominant source of d-Fe in aerosol particles deposited in the North Pacific Ocean (Fig. 7a). Nevertheless, the contribution of high-temp-FeOx, as a source of d-Fe in surface seawater during dust events, cannot be disregarded because the average fraction of non-crustal Fe during spring and dust events was 10.2 ± 7.6 %.

4.3.3. Crustal-Fe_{sol}% and anthro-Fe_{sol}%

The annual average crustal-Fe_{sol}% (ave.±1σ: 14.1 ± 9.3 %) was higher than the anthro-Fe_{sol}% (ave.±1σ: 9.35 ± 10.29 %) when the focus was on fine aerosol particles (Figs. 7c and 7d). This result is inconsistent with the finding of previous studies where the Fe_{sol}% of anthropogenic Fe derived from high-temperature combustion was higher than that of mineral dust (Sedwick et al., 2007; Sholkovitz et al., 2009). One of the reasons is that the Fe oxide nanoparticles were poorly solubilized at the aerosol pH of the samples obtained in this study. Marcotte et al. (2020) showed that the Fe_{sol}% of submicron Fe-oxides (<1.5 %) was lower than those of submicron illite and kaolinite (about 10 %). Similar results have been obtained from the experiments on Fe dissolution from aluminosilicates and Fe-oxides at pH 2.0 (particle diameter < 100 μm, Journet et al., 2008). According to the results of this study, the aerosol pH of fine aerosol particles with high Fe_{sol}% (>10 %) was lower than 3.0, but almost no fine aerosol samples whose aerosol pH was lower than 1.7 was observed (Fig. 4e). Therefore, even if the Fe-oxides were derived from high-temperature combustion, the significant increase in their anthro-$Fe_{sol\%}$ was unlikely without sufficient acidification. Another reason is that mineral dust with a low Fe_{sol}% was mainly present in coarse aerosol particles. The annual average of crustal-Fe_{sol}% in TSP was 6.52 ± 3.05 %, which was lower than that of anthro-Fe_{sol}%.

The crustal-Fe_{sol}% of fine aerosol particles in the 0.39–0.69 and 0.69–1.3 μm fractions were higher than that in the finest fraction throughout the year (Fig. 7c), which indicates that mineral dust in the 0.39–0.69 and 0.69–1.3 μm fractions was more aged than that in the finest fraction. This result is reasonable because internally mixed particles of Fe and sulfate were found in the fine aerosol particles, whose number fraction relative to the total number of Fe-bearing particles became the largest at around 700 nm rather than finer than 400 nm (Sullivan et al., 2007; Li et al., 2017; Zhu, Y. et al., 2020, 2022). The uptake of Fe-bearing particles into cloud water promotes internal mixing with sulfate (Li et al., 2017; Liu et al., 2018; Lin et al., 2019). However, the sufficient dissolution of Fe in fine aerosol particles at the pH condition of cloud water is unlikely (global average pH: 5.2, Shah et al., 2020), as observed in the relationship between aerosol pH and Fe_{sol}% (Fig. 4e). The aerosol pH decreased rapidly with the phase transition from cloud water to the aerosol concentration of protons in a tiny amount of aerosol liquid water content. Furthermore, the uptake coefficient of SO_2 by aluminosilicates increases as they experience cloud processes,

which is expected to further promotion of aerosol acidifications (Wang et al., 2019). Considering these facts, crustal-Fe_{sol}% in fine aerosol particles was enhanced by the aerosol–cloud water cycle during transport.

5. Implication for marine aerosol particles

The availability of the [d-Fe]/[d-Al] ratio for the evaluation of F_{crust} and F_{anthro} in marine aerosol particles was investigated using the observational results of previous studies (Buck et al., 2006, 2010b; Shelley et al., 2018; Baker et al., 2020; Sakata et al., 2022). In general, soluble metals in aerosol particles were extracted with ultrapure water through instantaneous or batch leaching, and only Baker et al. (2020) used ammonium acetate solution with pH 4.7. The [d-Fe]/[d-Al] ratio of the marine aerosol samples collected in the Pacific and Atlantic Oceans were rarely higher than 1.0 (Figs. 8a and 8b). The F_{anthro} of TSP collected from the Atlantic and Pacific Oceans were 9.58 % and 13.4 %, respectively (Fig. 8c). In the Pacific Ocean, F_{anthro} was higher in the region east of 170 °E because anthropogenic Fe in fine aerosol particles was transported farther than that in coarse mineral dust particles (Fig. 9a, Mahowald et al., 2018). By contrast, the large F_{anthro} in the Atlantic was detected around the coastal areas in North America and Europe (Fig. 9b). This result was consistent with the estimation of the F_{anthro} based on δ^{56}Fe, which indicated that more than half of the d-Fe in Fe around the coastal regions was derived from anthropogenic Fe with a negative δ^{56}Fe (Conway et al., 2019). However, the F_{anthro} of TSP with negative δ^{56}Fe values, which were estimated on the basis of the [d-Fe]/[d-Al] ratio, was 12.4 ± 2.9 % (Fig. 8c). Thus, the F_{anthro} estimated by the [d-Fe]/[d-Al] ratio differed from that estimated by δ^{56}Fe. One of the reasons for this discrepancy was the limited data of the [d-Fe]/[d-Al] and δ^{56}Fe ratios for emission source samples, specifically anthropogenic emissions. The [d-Fe]/[d-Al] ratio and δ^{56}Fe of high-temp-FeOx were estimated based on the measurement values of aerosol particles due to the lack of reliable reference materials for high-temp-FeOx. By contrast, the [d-Fe]/[d-Al] ratios of mineral dust and non-magnetic aluminosilicates of coal combustion and MSWI had a small effect on the uncertainty of F_{anthro} estimation due to the presence of reference values. Therefore, further studies involving the accumulated data on the [d-Fe]/[d-Al] ratio and δ^{56}Fe of high-temp-FeOx collected from various industrial sites are required. Currently, the accurate δ^{56}Fe and [d-Fe]/[d-Al] ratio of high-temp-FeOx may be obtained through the separation of magnetic particles, as performed by Zuo et al. (2022). The accumulated data on the previously reported values of [d-Fe]/[d-Al] ratio can be used and are expected to provide insights into the time-series variation in the contribution of anthropogenic Fe to aerosols in marine aerosols.

Figure 8b shows a scatter plot of the [d-Fe]/[d-Al] ratios and Fe_{sol}% of size-fractionated aerosol particles collected from the Atlantic and Pacific Oceans (Baker et al., 2020; Sakata et al., 2022). The average [d-Fe]/[d-Al] ratios of coarse and fine aerosol particles collected offshore of the Sahara Desert were 0.216 ± 0.163 and 0.155 ± 0.055, respectively. These values were similar to the [d-Fe]/[d-Al] ratio of Saharan dust (0.108 ± 0.061), which indicates that the d-Fe in these size-fractionated aerosol samples originated from Saharan dust. Iron in the size-fractionated aerosol particles collected in the western Pacific Ocean was also derived from mineral dust regardless of aerosol diameter because the EF of Fe in all size fractions was almost 1.00 (Sakata et al., 2022). The average [d-Fe]/[d-Al] ratio of coarse aerosol particles collected above the Pacific Ocean (0.378

± 0.104) was slightly higher than the average [d-Fe]/[d-Al] ratio of Asian dust (0.238 ± 0.201) but was similar to that of coarse aerosol particles collected in this study (0.408 ± 0.168). Therefore, the d-Fe in these samples was derived from the hydrolysis or proton-promoted dissolution of mineral dust. Although the Fe in coarse aerosol particles collected in the Atlantic and Pacific Oceans was derived from mineral dust, the [d-Fe]/[d-Al] ratios of the coarse and fine aerosol particles above the Atlantic Ocean were lower than that of coarse aerosol particles collected in the Pacific Ocean. The differences in mineralogical compositions of mineral dust in the hinterlands account for differences in the ratios of aerosol particles collected in the Atlantic and Pacific Oceans. Therefore, measurement of the [d-Fe]/[d-Al] ratio of soil samples around the sampling site is important to determine the representative [d-Fe]/[d-Al] ratio of mineral particles in aerosol particles.

The high Fe_{sol}% (>10 %) of fine aerosol particles in the Pacific was attributed to ferric organic complexes of humic-like substances (Fe(III)-HULIS, Sakata et al. 2022). The [d-Fe]/[d-Al] ratio of fine aerosol particles containing Fe(III)-HULIS was expected to be between 1.0 and 1.5 due to ligand-promoted dissolution. However, the obtained [d-Fe]/[d-Al] ratio for these particles was 0.440 ± 0.117 (range: 0.255–0.567), which was consistent with the ratio of Asian dust that underwent proton-promoted dissolution. A previous study reported that aerosol acidification of aluminosilicates enhanced the Fe_{sol}% of samples; Fe(III)-HULIS then formed via complexation reactions in cloud water (Sakata et al., 2022). The [d-Fe]/[d-Al] ratio may not change even if the Fe species was altered by atmospheric processes after Fe solubilization. However, further investigation of this point is required. Moreover, to evaluate source and dissolution processes using the [d-Fe]/[d-Al] ratio, we preferred the determination of the [d-Fe]/[d-Al] ratio via ultrapure water extraction without organic ligands (e.g., oxalate and acetate) because the ratio is altered if the extracted solution contains organic ligands (e.g., coarse aerosol (P) versus coarse aerosol (L), Fig. 6a). The data on the [d-Fe]/[d-Al] ratio of size-fractionated marine aerosol particles under the effect of high-temp-FeOx up to this point have not been published. Therefore, further studies on the [d-Fe]/[d-Al] ratio of marine aerosol particles influenced by high-temp-FeOx are required. If future studies detect high [d-Fe]/[d-Al] ratios in marine aerosol samples that are strongly affected by high-temp-FeOx, then the [d-Fe]/[d-Al] ratio will be a powerful tool for estimation of the fraction of crustal and non-crustal Fe in d-Fe in marine aerosol particles.

6. Conclusion

Annual observations of the total and d-Fe and Al concentrations in size-fractionated aerosol particles were conducted at the eastern end of East Asia. The total Fe and Al concentrations were mainly distributed in coarse aerosol particles, whereas d-Fe and d-Al concentrations dominated fine aerosol particles. Given the higher d-Fe concentration and longer residence time of fine aerosol particles than coarse aerosol particles, the atmospheric deposition of fine aerosol particles was the dominant source of d-Fe in the surface ocean. The [d-Fe]/[d-Al] ratio of coarse aerosol particles (0.408 ± 0.168) was lower than that of fine aerosol particles (1.15 ± 0.80). Thus, the sources of d-Fe differed between coarse and fine aerosol particles. The [d-Fe]/[d-Al] ratio of coarse aerosol particles was similar to that observed for Fe dissolved via proton-promoted dissolution. The Fe_{sol}% increased as the surfaces of coarse particles became hygroscopic through the reaction with sulfuric acid. This effect intensified

with the reduction in particle size. The fine aerosol particles presented a wide range of [d-Fe]/[d-Al] ratios (0.386–4.67). The correlation of the [d-Fe]/[d-Al] ratio of the fine aerosol particles with the EF of Fe indicated that the high [d-Fe]/[d-Al] ratios (>1.5) can be attributed to non-crustal Fe. High-temp FeOx in magnetic particles were likely the dominant species of non-crustal Fe with high [d-Fe]/[d-Al] ratios. The F_{crust} and F_{anthro} were evaluated using the [d-Fe]/[d-Al] ratios in aerosol particles and their emission source samples. Approximately 80 % of d-Fe in TSP collected in spring, when numerous aerosol transport events from East Asia to the North Pacific occurred, originated from mineral particles. The high F_{crust} was attributed to the higher crustal-Fe_{sol}% than anthro-Fe_{sol}%. The Fe_{sol}% of submicron mineral dust (e.g., illite) was higher than those of hematite and magnetite of the same size in solutions with pH higher than 1.7. Furthermore, the Fe_{sol}% of fine aerosol particles increased with the decrease in aerosol pH, which indicates that the acidification of mineral particles played an important role in the supply of d-Fe to surface seawater in the North Pacific via atmospheric deposition. Thus, the source estimation of d-Fe using the [d-Fe]/[d-Al] ratio is a powerful tool for estimation not only of the source of d-Fe in marine aerosols but also the dissolution processes of Fe in aerosol particles. The source estimation of d-Fe using the [d-Fe]/[d-Al] ratio also has the advantage of being performed through a simple analytical method, in which Fe and Al are extracted by ultrapure water, and their concentrations are measured through ICP–MS. Therefore, this method can be easily conducted not only in future studies but also on aerosol samples collected in previous research. Currently, data on the [d-Fe]/[d-Al] ratios of aerosols, which are strongly affected by anthropogenic Fe and emission sources associated with high-temperature combustion processes, are limited. Therefore, collection of data on the [d-Fe]/[d-Al] ratios of these samples will enable us to identify the emission sources of d-Fe in marine aerosol particles with increased robustness.

Data Availability All quantitative data will be available at the ERAN database (https://www.ied.tsukuba.ac.jp/database/00156.html) with a doi: 10.34355/CRiED.U.Tsukuba.00156.

Supplement. The supplement related to this article is available online at XXXX.

Author contributions. The study was designed by K.S., A.S., and Y.T. Aerosol sampling was performed by K.S. and Y.Y. Major ion concentrations were determined by K.S., Y.Y., and C.M. Trace metal concentrations were measured by K.S., C.M., and M.K. The paper was written by K.S., and Y.T., and all authors were reviewed the manuscript before submission.

***Competing interests*.** The authors declare that they have no conflict of interest.

Financial support. The studies were supported by Grant-in-Aid for JSPS Research Fellow (14J06437).

Figure captions

Figure 1: Sites (Higashi-Hiroshima) of size-fractionated aerosol sampling. Maps were visualized by Ocean Data View (Schlitzer, 2021).

Figure 2: Monthly variations and size distributions of the (a) total Al and (b) total Fe concentrations. (c) Box plot of EF in each size fraction.

Figure 3: Monthly variation and size distributions of (a) d-Fe and (b) Fe_{sol}%. (c) Box plot of Fe_{sol}% in each size fraction. Monthly variation and size distributions of (d) d-Al and (e) Al_{sol}%. (f) Box plot of Al_{sol}% in each size fraction.

Figure 4: Scatter plots of Fe_{sol}% and Al_{sol}% in coarse aerosol particles with (a) [nss-SO_4^{2-}]/[total Fe] and [nss-SO_4^{2-}]/[total Al] and (b) [NO_3^-]/[total Fe] and [NO_3^-]/[total Al]. Scatter plots of Fe_{sol}% and Al_{sol}% in fine aerosol particles with (c) [nss-SO_4^{2-}]/[total Fe] and [nss-SO_4^{2-}]/[total Al] , (d) [NO_3^-]/[total Fe] and [NO_3^-]/[total Al] and (e) aerosol pH.

Figure 5: Scatter plots of d-Fe with (a) non-crustal Fe, (b) total V, (c) total Cu, (d) total Sb, and (e) total Pb concentrations in fine aerosol particles.

Figure 6: (a) Box plot of [d-Fe]/[d-Al] in emission source samples (Proton) and (Ligand) indicating proton- and ligand-promoted dissolutions. Scatter plots of the [d-Fe]/[d-Al] ratio with (b) the Fe_{sol}% and (c) EF of Fe. Light blue circles and black squares in panels (b) and (c) represent the data on coarse and fine aerosol particles collected in Higashi-Hiroshima, respectively. Pink, yellow, light green, and gray regions show the typical ranges of the [d-Fe]/[d-Al] ratios of aluminosilicate glasses of coal combustion and MSWI, the proton- and ligand-promoted dissolution of mineral dust, and high-temp-FeOx, respectively. The regions were decided based on the box plots of panels (a).

Figure 7: Monthly variations of (a) non-crustal Fe fraction in TSP and (b) non-crustal Fe fraction in fine aerosol particles, (c) crustal-Fe_{sol}%, and (d) non-crustal Fe_{sol}% when the [d-Fe]/[d-Al] ratio of non-crustal Fe is 2.08. The yellow shaded region shows the period when the air mass was mainly derived from Japan.

Figure 8: Scatter plots of the [d-Fe]/[d-Al] ratio with Fe_{sol}% in (a) TSP samples and (b) size-fractionated aerosol particles collected in the marine atmosphere. (c) The fraction of non-crustal d-Fe in these samples was calculated using Equations 6 and 7. The [d-Fe]/[d-Al] ratios of mineral dust in the Pacific and Atlantic Oceans were the average ratios of Asian (0.238) and Saharan dusts (0.163), respectively. The [d-Fe]/[d-Al] ratio of non-crustal Fe was fixed at 2.08. The [d-Fe]/[d-Al] ratios of the TSP and size-fractionated aerosol samples were adapted from the works of Buck et al. (2006, 2010b), Shelley et al. (2018), Baker et al. (2020), and Sakata et al. (2022). The Fe isotopic ratio of TSP in the Atlantic Ocean was reported by Conway et al. (2019). Pink, yellow, light green, and gray regions in panels (a) and (b) show the typical [d-Fe]/[d-Al] ratios of coal/MSWI fly ash, proton- and ligand-promoted mineral dust dissolutions, and pyrogenic Fe oxides, respectively.

Figure 9: Non-crustal Fe fractions in the TSP samples collected from (a) the Pacific Ocean and (b) Atlantic Ocean. Non-crustal Fe fractions were calculated using the [d-Fe]/[d-Al] ratios reported by Buck et al. (2006, 2010b) and Shelley et al. (2018). The figures were described by Ocean Data View (Schlitzer, 2021).

Figures

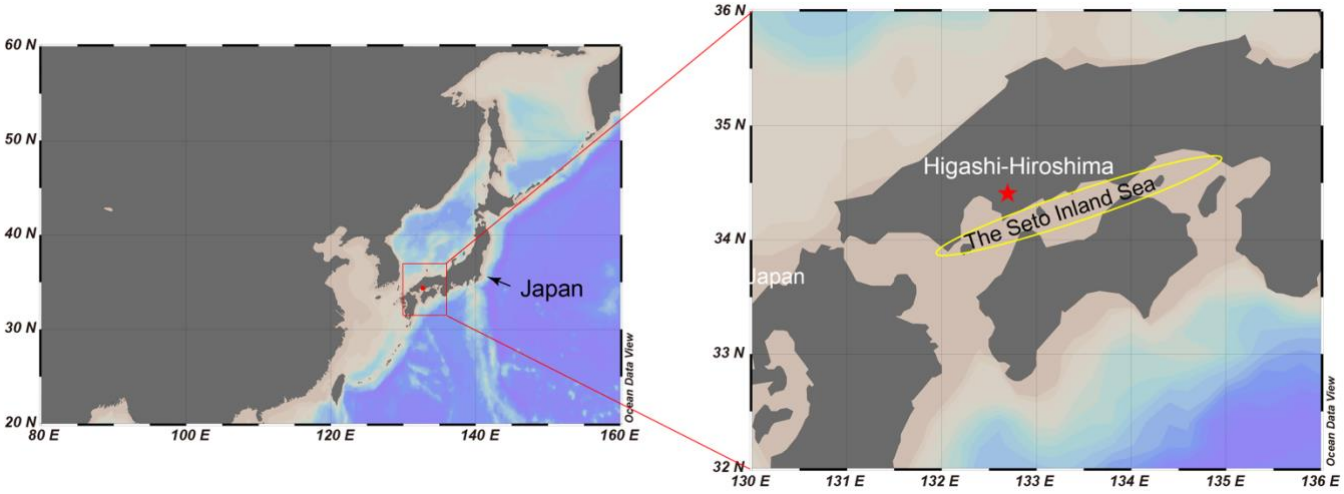

Figure 1: Sites (Higashi-Hiroshima) of size-fractionated aerosol sampling. Maps were visualized by Ocean Data View (Schlitzer, 2021).

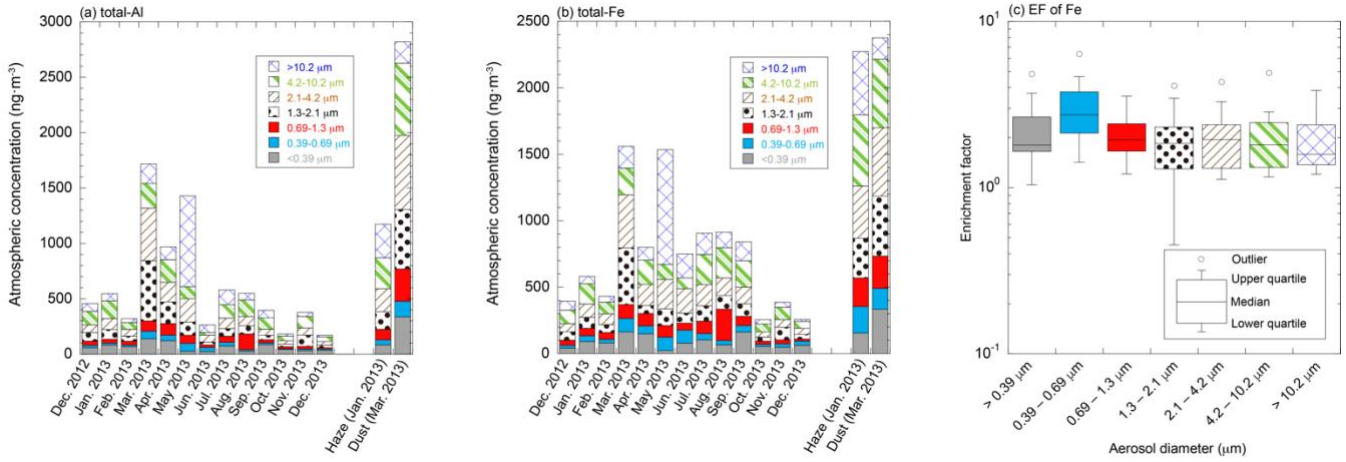

Figure 2: Monthly variations and size distributions of the (a) total Al and (b) total Fe concentrations. (c) Box plot of EF in each size fraction.

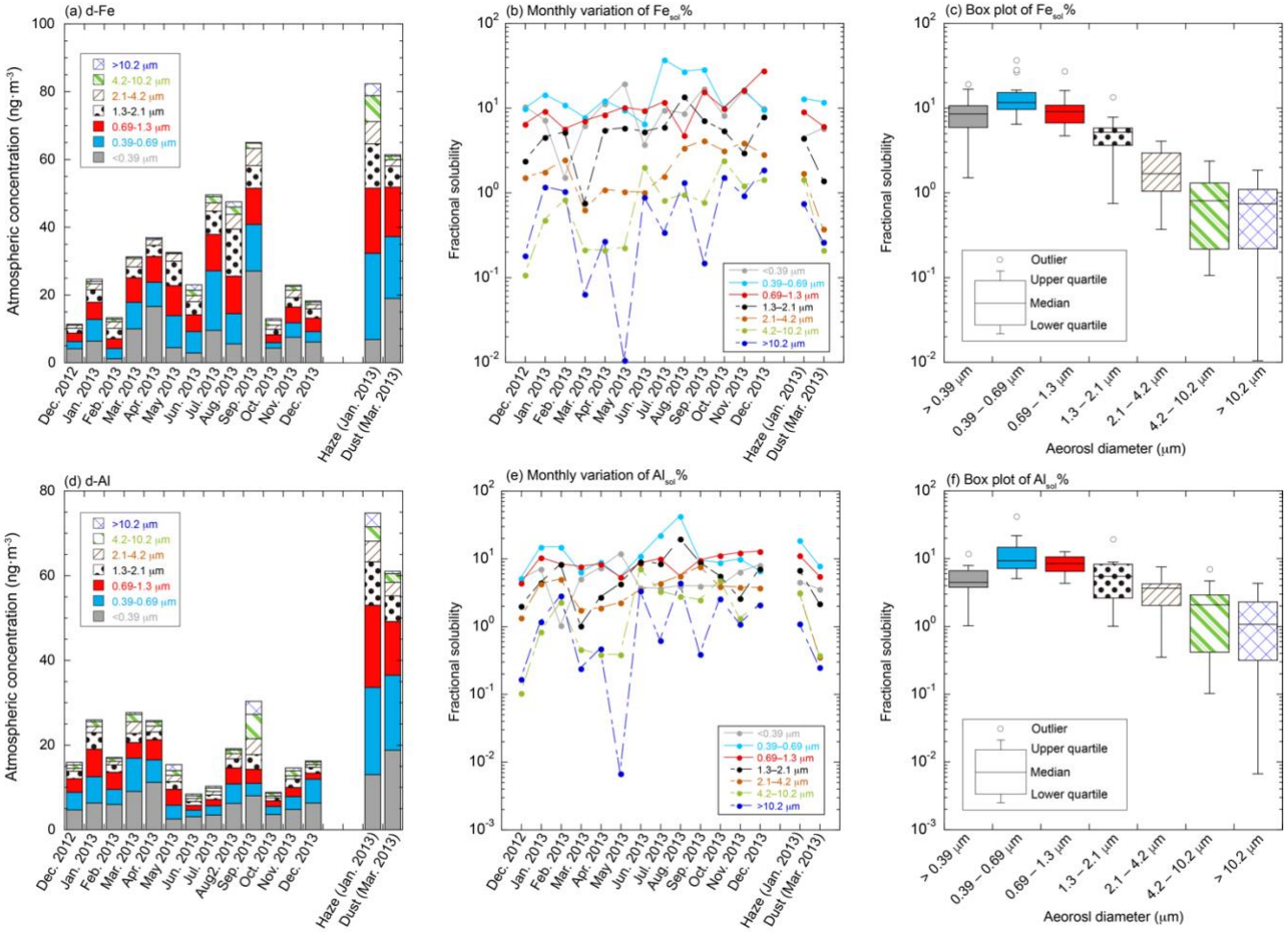

Figure 3: Monthly variation and size distributions of (a) d-Fe and (b) Fe_{sol}%. (c) Box plot of Fe_{sol}% in each size fraction. Monthly variation and size distributions of (d) d-Al and (e) Al_{sol}%. (f) Box plot of Al_{sol}% in each size fraction.

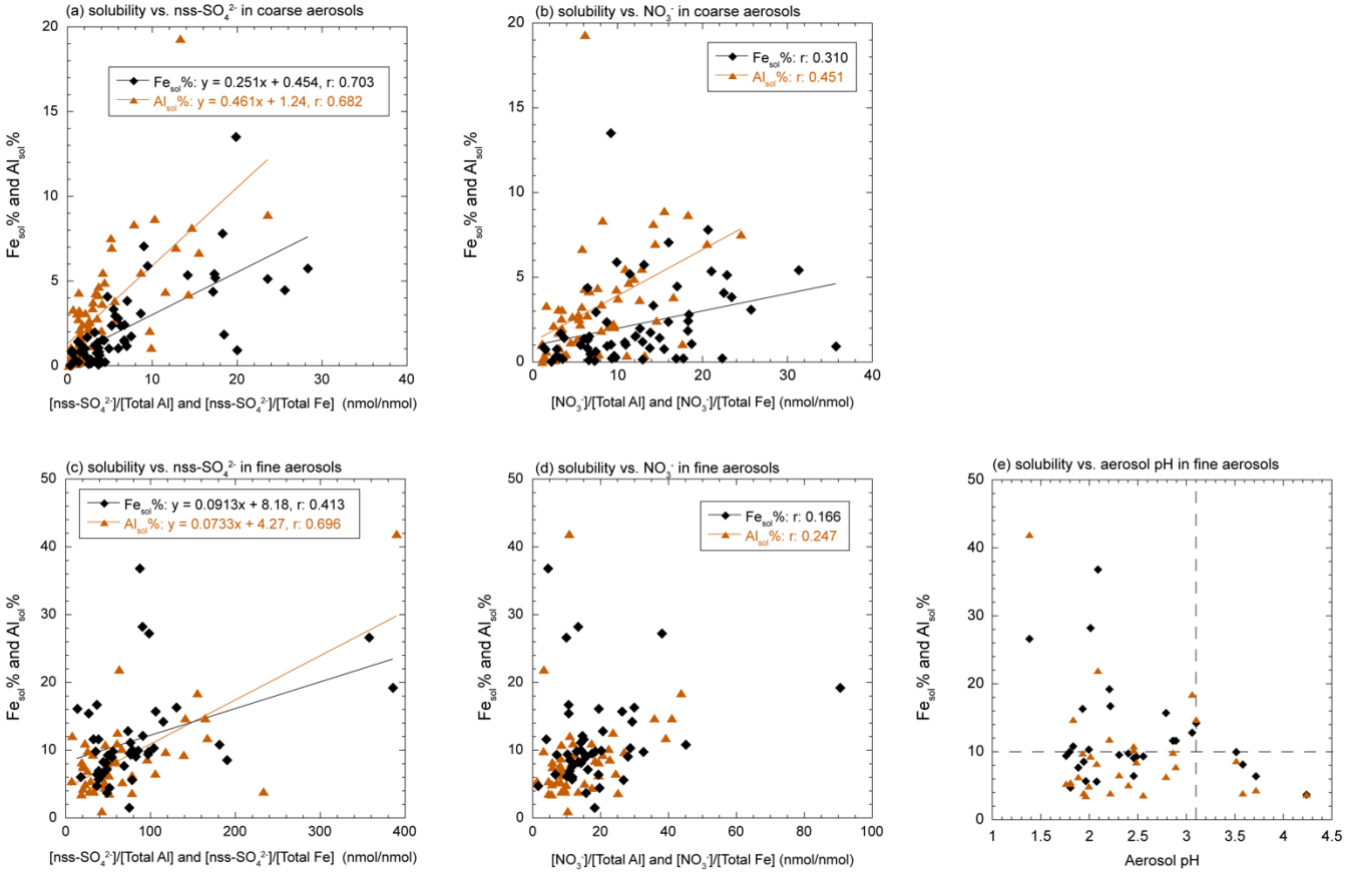

Figure 4: Scatter plots of Fe_{sol}% and Al_{sol}% in coarse aerosol particles with (a) [nss-SO_4^{2-}]/[total Fe] and [nss-SO_4^{2-}]/[total Al] and (b) [NO_3^-]/[total Fe] and [NO_3^-]/[total Al]. Scatter plots of Fe_{sol}% and Al_{sol}% in fine aerosol particles with (c) [nss-SO_4^{2-}]/[total Fe] and [nss-SO_4^{2-}]/[total Al] , (d) [NO_3^-]/[total Fe] and [NO_3^-]/[total Al] and (e) aerosol pH.

690

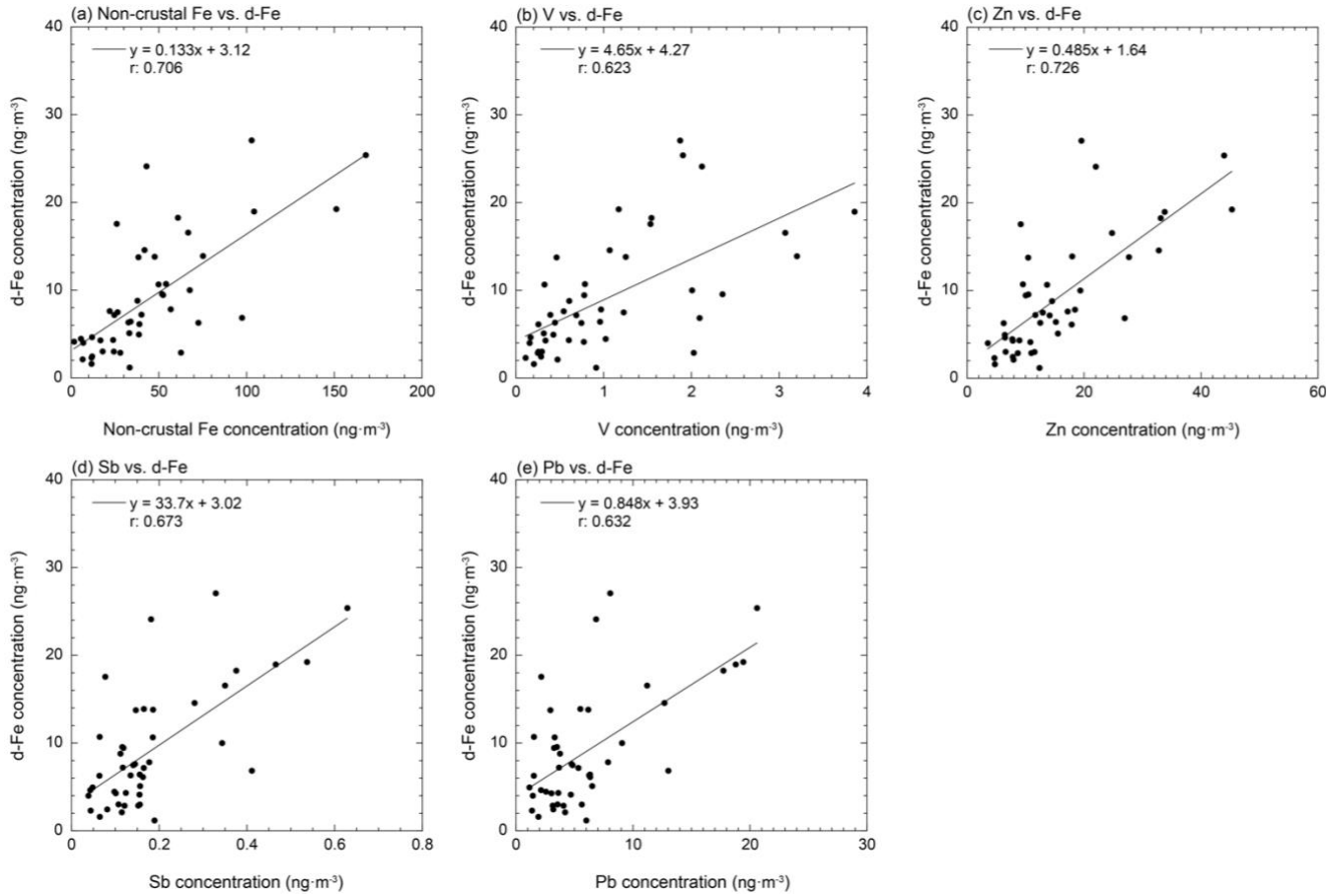

Figure 5: Scatter plots of d-Fe with (a) non-crustal Fe, (b) total V, (c) total Cu, (d) total Sb, and (e) total Pb concentrations in fine aerosol particles.

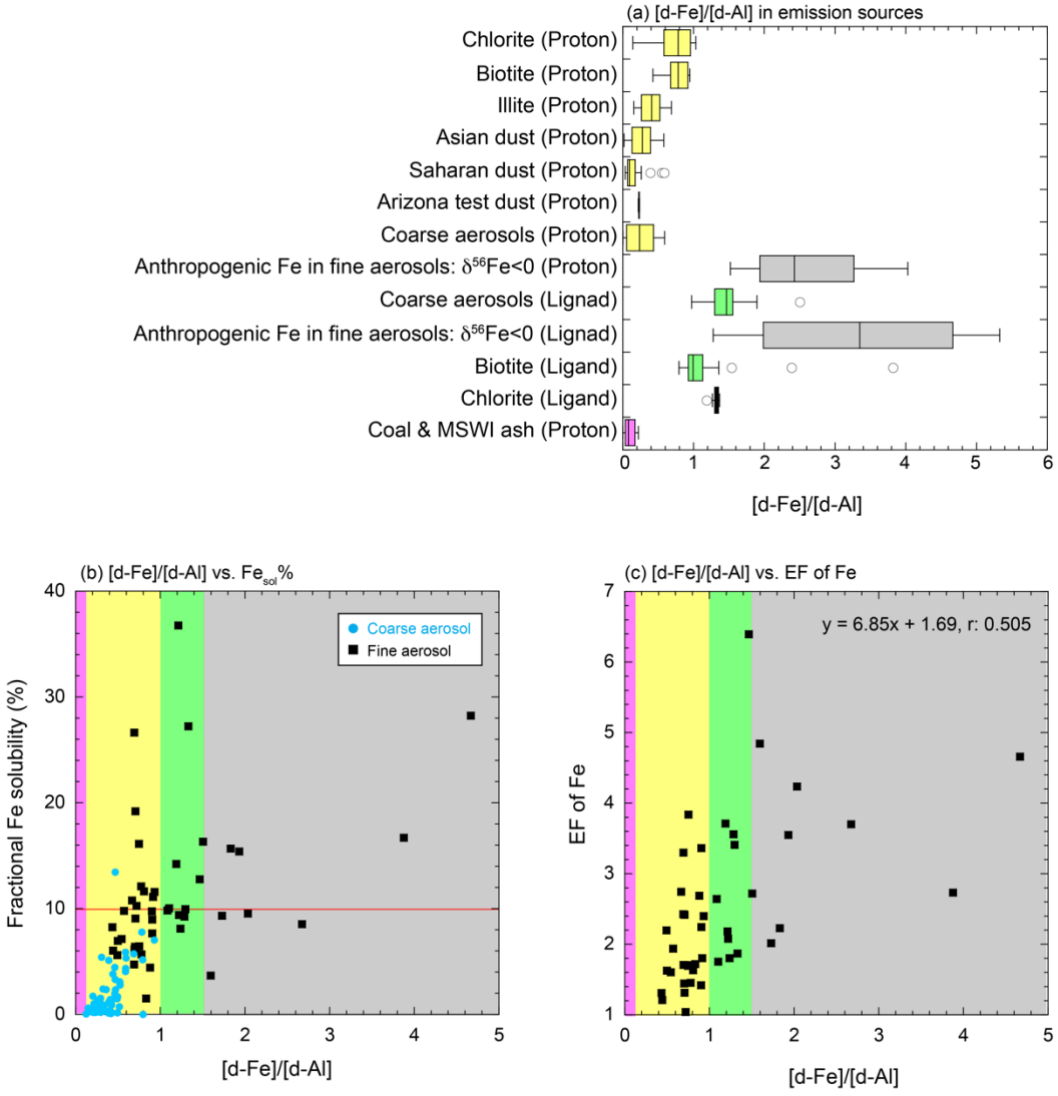

Figure 6: (a) Box plot of [d-Fe]/[d-Al] in emission source samples (Proton) and (Ligand) indicating proton- and ligand-promoted dissolutions. Scatter plots of the [d-Fe]/[d-Al] ratio with (b) the Fe_{sol}% and (c) EF of Fe. Light blue circles and black squares in panels (b) and (c) represent the data on coarse and fine aerosol particles collected in Higashi-Hiroshima, respectively. Pink, yellow, light green, and gray regions show the typical ranges of the [d-Fe]/[d-Al] ratios of aluminosilicate glasses of coal combustion and MSWI, the proton- and ligand-promoted dissolution of mineral dust, and high-temp-FeOx, respectively. The regions were decided based on the box plots of panels (a).

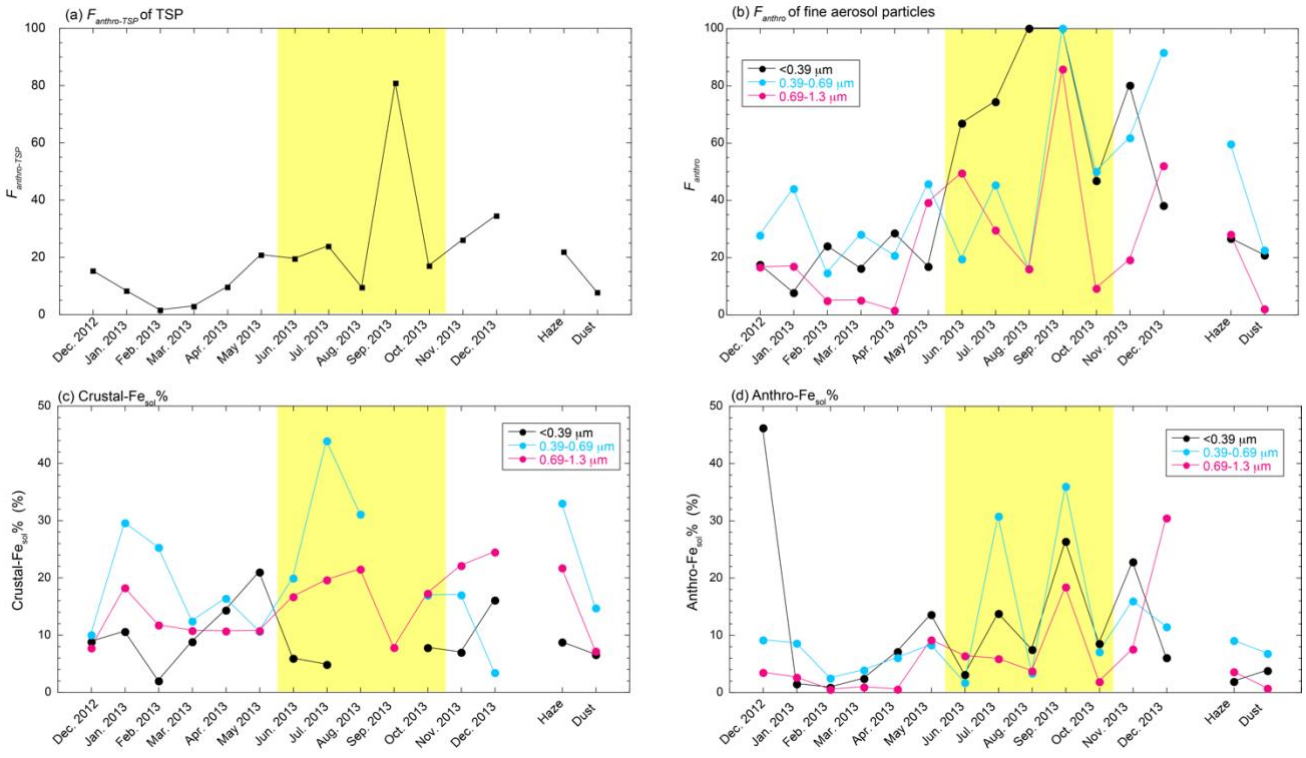

Figure 7: Monthly variations of (a) non-crustal Fe fraction in TSP and (b) non-crustal Fe fraction in fine aerosol particles, (c) crustal-Fe_{sol}%, and (d) non-crustal Fe_{sol}% when the [d-Fe]/[d-Al] ratio of non-crustal Fe is 2.08. The yellow shaded region shows the period when the air mass was mainly derived from Japan.

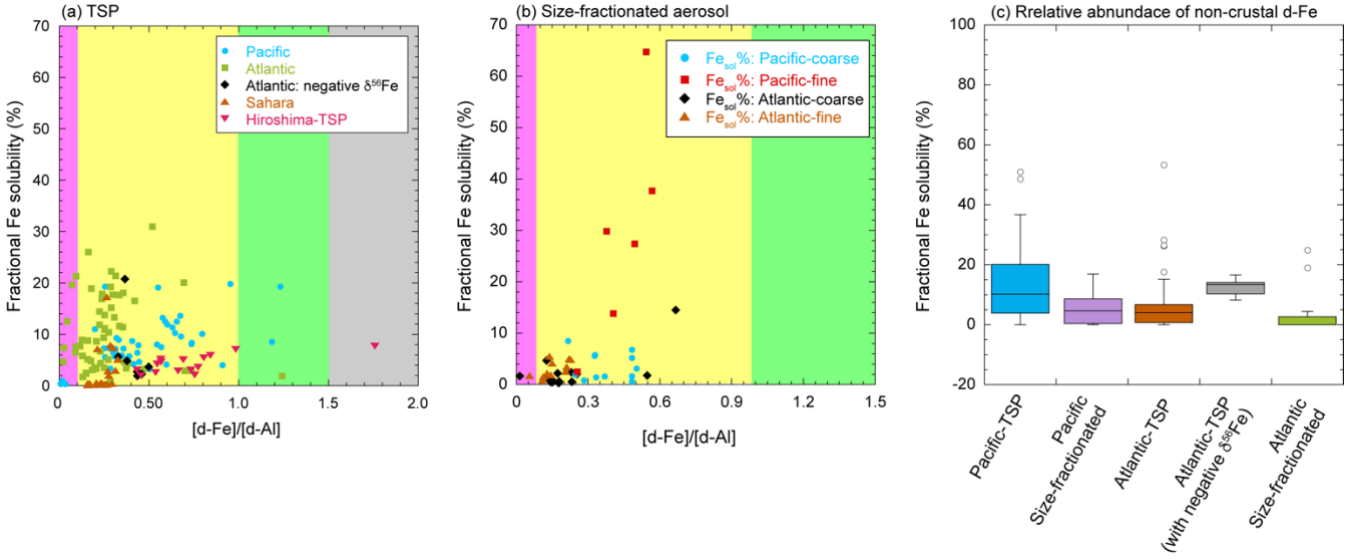

Figure 8: Scatter plots of the [d-Fe]/[d-Al] ratio with Fe_{sol}% in (a) TSP samples and (b) size-fractionated aerosol particles collected in the marine atmosphere. (c) The fraction of non-crustal d-Fe in these samples was calculated using Equations 6 and 7. The [d-Fe]/[d-Al] ratios of mineral dust in the Pacific and Atlantic Oceans were the average ratios of Asian (0.238) and Saharan dusts (0.163), respectively. The [d-Fe]/[d-Al] ratio of non-crustal Fe was fixed at 2.08. The [d-Fe]/[d-Al] ratios of the TSP and size-fractionated aerosol samples were adapted from the works of Buck et al. (2006, 2010b), Shelley et al. (2018), Baker et al. (2020), and Sakata et al. (2022). The Fe isotopic ratio of TSP in the Atlantic Ocean was reported by Conway et al. (2019). Pink, yellow, light green, and gray regions in panels (a) and (b) show the typical [d-Fe]/[d-Al] ratios of coal/MSWI fly ash, proton- and ligand-promoted mineral dust dissolutions, and pyrogenic Fe oxides, respectively.

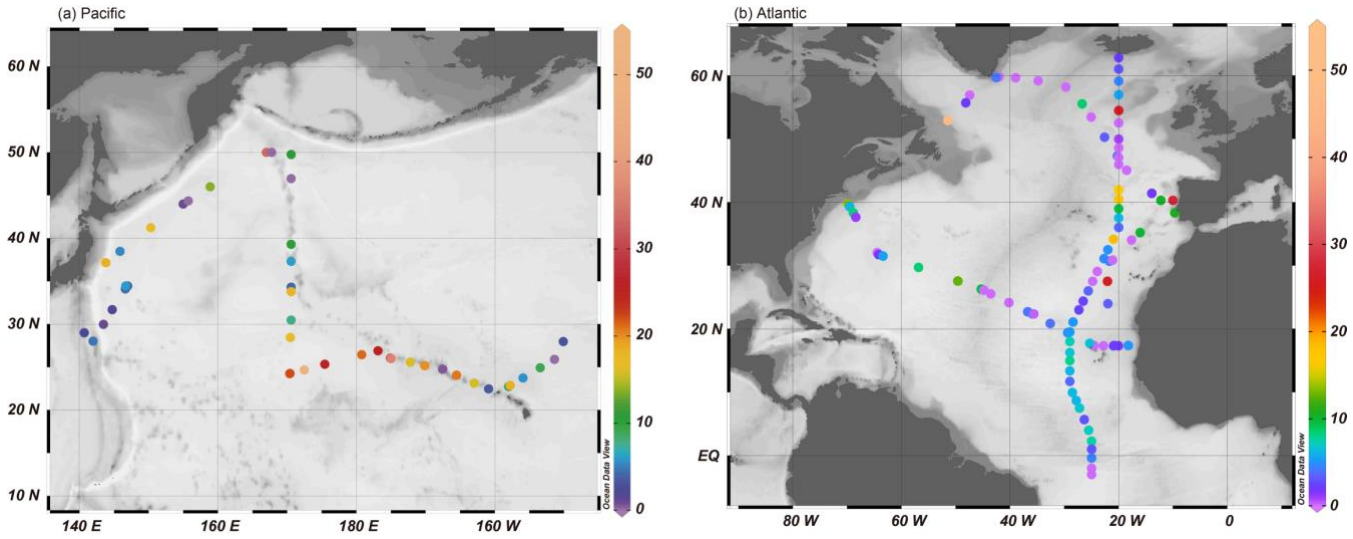

Figure 9: Non-crustal Fe fractions in the TSP samples collected from (a) the Pacific Ocean and (b) Atlantic Ocean. Non-crustal Fe fractions were calculated using the [d-Fe]/[d-Al] ratios reported by Buck et al. (2006, 2010b) and Shelley et al. (2018). The figures were described by Ocean Data View (Schlitzer, 2021).

References

Acker, J. G., Bricker, O. P.: The influence of pH on biotite dissolution and alteration kinetics at low temperature, Geochim. Cosmochim. Acta, 56, 3073–3092, https://doi.org/10.1016/0016-7037(92)90290-Y, 1992.

Adachi, K., Tainosho, Y.: Characterization of heavy metal particles embedded in tire dust, Environ. Int., 30, 1009–1017, https://doi.org/10.1016/j.envint.2004.04.004, 2004.

Akita, S., Maeda, T., Takeuchi, H.: Recovery of vanadium and nickel in fly ash from heavy oil, J. Chem., Tech. Biotechnol., 62, 345–350, https://doi.org/10.1002/jctb.280620406, 1995.

Baker, A. R., and Jickells, T. D.: Atmospheric deposition of soluble trace elements along the Atlantic Meridional Transect (AMT), Prog. Oceanogr., 158, 41–51, http://dx.doi.org/10.1016/j.pocean.2016.10.002, 2017.

Baker, A. R., and Jickells, T. D.: Mineral particle size as a control on aerosol iron solubility, Geophys. Res. Lett., 33, L17608, https://doi.org/10.1029/2006GL026557, 2006.

Baker, A. R., Li, M., Chance, R.: Trace metal fractional solubility in size-segregated aerosols from the tropical eastern Atlantic Ocean, Global Biogeochm. Cy., 34, e2019GB006510, https://doi.org/10.1029/2019GB006510, 2020.

Bibi, I., Singh, B., and Silvester, E.: Dissolution of illite in saline-acidic solutions at 25 ºC, Geochim. Cosmochim. Acta, 75, 3237–3249, https://doi.org/10.1016/j.gca.2011.03.022, 2011.

Boyd, P. W., Jickells, T., Law, C. S., Blain, S., Boyle, E. A., Buesseler, K. O., Coale, K. H., Cullen, J. J., de Beear, H. J. W., Follows, M., Harvey, M., Lancelot, C., Levasseur, M., Owens, N. P. J., Pollard, R., Rivkin, R. B., Sarmiento, J., Schoemann, V., Smetacek, V., Takeda, S., Tsuda, A., Turner, S., and Watson, A. J.: Mesoscale iron enrichment experiments 1993–2005: Synthesis, and future directions, Science, 315, 612–617, https://doi.org/10.1126/science.1131669, 2007.

Brantley, S. L., Kubicki, J. D., White, A. F.: Kinetics of water-rock interaction, Springer, New York, https://doi.org/10.1007/978-0-387-73563-4, 2008.

Bray, A. W., Oelkers, E. H., Bonneville, S., Wolff-Boenisch, D., Potts, N. J., Fones, G., and Benning, L. G.: The effect of pH, grain size, and organic ligands on biotite weathering rates, Geochim. Cosmochim. Acta, 164, 127–145, http://dx.doi.org/10.1016/j.gca.2015.04.048, 2015.

Buck, C. S., Landing, W. M., and Resing, J.: Pacific Ocean aerosols: Deposition and solubility of iron, aluminum, and other trace elements, Mar. Chem., 157, 117–130, http://dx.doi.org/10.1016/j.marchem.2013.09.005, 2013.

Buck, C. S., Landing, W. M., and Resing, J.: Particle size and aerosol iron solubility: A high-resolution analysis of Atlantic aerosols, Mar. Chem., 120, 14–24, https://doi.org/10.1016/j.marchem.2008.11.002, 2010a.

Buck, C. S., Landing, W. M., Resing, J. A. and Lebon, G. T.: Aerosol iron and aluminum solubility in the northwest Pacific Ocean: Results from the 2002 IOC cruise, Geochem. Geophys. Geosyst., 7, 4, Q04M07, https://doi.org/10.1029/2005GC000977, 2006.

Buck, C. S., Landing, W. M., Resing, J. A., Measures, C. I.: The solubility and deposition of aerosol Fe and other trace elements in the North Atlantic Ocean: Observations from the A16N CLIVAR/CO_2 repeat hydrography section, Mar. Chem., 120, 57–70, https://doi.org/10.1016/j.marchem.2008.08.003, 2010b.

Cao, J. J., Chow, J. C., Watson, J. G., Wu, F., Han, Y. M., Jin, Z. D., Shen, Z. X., An, Z. S.: Size-differentiated source profiles for fugitive dust in the Chinese Loess Plateau, Atmos. Environ., 42, 2261–2275, https://doi.org/10.1016/j.atmosenv.2007.12.041, 2008.

Chance, R., Jickells, T. D., and Baker, A. R.: Atmospheric trace metal concentrations, solubility and deposition fluxes in remote marine air over the south-east Atlantic. Mar. Chem., 177, 45–56, http://dx.doi.org/10.1016/j.marchem.2015.06.028, 2015.

Chang, C. Y., Wang, C. F., Mui, D. T., Chiang, H. L.: Application of methods (sequential extraction procedures and high-pressure digestion method) to fly ash particles to determine the element constituents: A case study for BCR-176. J. Hazard. Mater., 163, 578–587, https://doi.org/10.1016/j.jhazmat.2008.07.039, 2009.

Chen, H. and Grassian, V. H.: Iron dissolution of dust source materials during simulated acidic processing: The effect of sulfuric, acetic, and oxalic acids, Environ. Sci. Technol., 47, 1031210321, https://doi.org/10.1021/es401285s, 2013.

Clegg, S. L., Pitzer, K. S., and Brimblecombe, P.: Thermodynamics of multicomponent, miscible, ionic solutions. II. Mixtures including unsymmetrical electrolyte. J. Phys. Chem., 96**,** 9470–9479, https://doi.org/10.1021/j100202a074, 1992.

Conway, T. M., Hamilton D. S., Shelley, R. U., Aguilar-Islas, A. M., Landing, W. M., Mahowald, N. ., and John, S. G.: Tracing and constraining anthropogenic aerosol iron fluxes to the North Atlantic Ocean using iron isotopes, Nature Commun., 10, 2628, https://doi.org/10.1038/s41467-019-10457-w, 2019.

Czech, T., Morphology and chemical composition of magnetic particles separated from coal fly ash, Materials, 15, 528, https://doi.org/10.3390/ma15020528, 2022.

Desboeufs, K. V., Losno, R., Colin, J. L.: Factors influencing aerosol solubility during cloud processes, Atmos. Environ., 35, 3529–3537, https://doi.org/10.1016/S1352-2310(00)00472-6, 2001.

Ding, Z. L., Sun, J. M., Yang, S. L., Liu, T. S.: Geochemistry of the Pliocene red clay formation in the Chinese Loess Plateau and implications for its origin, source provenance and paleoclimate change, Geochim. Cosmochim. Acta, 65, 6, 901–913, https://doi.org/10.1016/S0016-7037(00)00571-8, 2001.

Duvall, R. M., Majestic, B. J., Shafer, M. M., Chuang, P. Y., Simoneit, B. R. T. Schauer, J. J.: The water-soluble fraction of carbon, sulfur, and crustal elements in Asian aerosols and Asian soils, Atmos. Environ., 42, 5872–5884, https://doi.org/10.1016/j.atmosenv.2008.03.028, 2008.

Falkowski, P., Scholes, R. J., Boyle, E., Canadell, J., Canfield, D., Elser, J., Gruber, N., Hibbard, K., Hogberg, P., Linder, S., Mackenzie, F. T., Moore, B., Pedersen, T., Rosenthal, Y., Seitzinger, S., Smetacek, V., and Steffen, W.: The global carbon cycle: A test of our knowledge of earth as a system, Science, 290, 291–296, https://doi.org/10.1126/science.290.5490.291, 2000.

Fang, T., Guo, H., Zeng, L., Verma, V., Nenes, A., and Weber, R.: Highly Acidic Ambient Particles, Soluble Metals, and Oxidative Potential: A Link between Sulfate and Aerosol Toxicity, Environ. Sci. Technol., 51, 2611–2620, https://doi.org/10.1021/acs.est.6b06151, 2017.

Fitzgerald, E., Ault, A. P., Zauscher, M. D., Mayol-Bracero, O. L., and Prather, K. A.: Comparison of the mixing state of long-range transported Asian and African mineral dust, Atmos. Environ., 115, 19–25, https://doi.org/10.1016/j.atmosenv.2015.04.031, 2015.

Fomenko, E. V., Anshits, N. N., Solovyov, L. A., Knyazev, Y. V., Semenov, S. V., Bayukov, O. A., Anshits, A. G.: Magnetic fractions of $PM_{2.5}$, $PM_{2.5–10}$, PM_{10} from coal fly ash as environmental pollutants, ACS Omega, 6, 20076–20085, https://doi.org/10.1021/acsomega.1c03187, 2021.

Friese, E., and Ebel, A.: Temperature dependent thermodynamic model of the system H^+–NH_4^+–Na^+–SO_4^{2-}–NO_3^-–Cl^-–H_2O. J. Phys. Chem. A, 114, 11595–11631, https://doi.org/10.1021/jp101041j, 2010.

Furuya, K., Miyajima, Y., Chiba, T., Kikuchi, T.: Elemental characterization of particle size-density separated coal fly ash by spectrophotometry, inductively coupled plasma emission spectrometry, and scanning electron microscopy-energy dispersive X-ray analysis. Environ. Sci. Technol., 21, 898–903, https://doi.org/10.1021/es00163a008, 1987.

Gao, Y., Marsay, C. M., Yu, S., Fan, S., Mukherjee, P., Buck, C. S., Landing, W. M.: Particle-size variability of aerosol iron and impact on iron solubility and dry deposition fluxes to the Arctic Ocean, Sci. Rep., 9, 16653, https://doi.org/10.1038/s41598-019-52468-z, 2019.

Gietl, J. K., Lawrence, R., Thorpe, A. J., Harrison, R. M.: Identification of brake wear particles and derivation of a quantitative tracer for brake dust at a major road. Atmos. Environ., 44, 141–146, https://doi.org/10.1016/j.atmosenv.2009.10.016, 2010.

Gitari, W. M., Fatoba, O. O., Petrik, L. F., Vadapalli, V. R. K.: Leaching characteristics of selected south African fly ashes: Effect of pH on the release of major and trace species, J. Environ. Sci. Health A, 44, 206–220, https://doi.org/10.1080/10934520802539897, 2009.

Guo, H., Nenes, A., Weber, R. J.: The underappreciated role of nonvolatile cations in aerosol ammonium-sulfate molar ratios. Atmos. Chem. Phys., 18, 17307–17323, https://doi.org/10.5194/acp-18-17307-2018, 2018

Halle, L. L., Palmqvist, A., Kampmann, K., Jensen, A., Hansen, T., Khan, F. R.: Tire wear particle and leachate exposures from a pristine and road-worn tire to *Hyalella azteca*: Comparison of chemical content and biological effects, Aquat. Toxicol., 232, https://doi.org/10.1016/j.aquatox.2021.105769, 2021.

Hansen, L. D., Silberman, D., Fisher, G. L.: Crystalline components of stack-collected, size-fractionated coal fly ash, Environ. Sci. Technol., 15, 1057–1062, https://doi.org/10.1021/es00091a004, 1981.

Harrison, R. M., Allan, J., Carruthers, D., Heal, M. R., Lewis, A. C., Marner, B., Murrells, T., Williams, A.: Non-exhaust vehicle emissions of particulate matter and VOC from road traffic: A review, Atmos. Environ., 262, 118592, https://doi.org/10.1016/j.atmosenv.2021.118592, 2021.

Hsieh, C. C., Chen, H. Y., and Ho, T. Y.: The effect of aerosol size on Fe solubility and deposition flux: A case study in the East China Sea. Mar. Chem., 241, 104106, https://doi.org/10.1016/j.marchem.2022.104106, 2022.

Huang, S. J., Chang, C. Y., Mui, D. T., Chang, F. C., Lee, M. Y., Wang, C. F.: Sequential extraction for evaluating the leaching behavior of selected elements in municipal solid waste incineration fly ash. J. Hazard. Mater., 149, 180–188, https://doi.org/10.1016/j.jhazmat.2007.03.067, 2007.

Iijima, A., Sato, K., Yano, K., Tago, H., Kato, M., Kimura, H., Furuta, N.: Particle size and composition distribution analysis of automotive brake abrasion dusts for the evaluation of antimony sources of airborne particulate matter, Atmos. Environ., 41, 4908–4919, https://doi.org/10.1016/j.atmosenv.2007.02.005, 2007.

Ito, A., and Shi, Z.: Delivery of anthropogenic bioavailable iron from mineral dust and combustion aerosols to the ocean, Atmos. Chem. Phys., 16, 85–99, https://doi.org/10.5194/acp-16-85-2016, 2016.

Ito, A., Myriokefalitakis, S., Kanakidou, M., Mahowald, N. M., Scanza, R. A., Hamilton, D. S., Baker, A. R., Jickells, T., Sarin, M., Bikkina, S., Gao, Y., Shelley, R. U., Buck, C. S., Landing, W. M., Bowie, A. R., Perron, M. M. G., GUieu, C., Meskhidze, N., Johnson, M. S., Feng, Y., Kok, J. F., Nenes, A., Duce, R. A.: Pyrogenic iron: The missing link to high iron solubility in aerosols. Sci. Adv., 5, eaau7671, https://doi.org/10.1126/sciadv.aau7671, 2019.

Ito, A., Ye, Y., Baldo, C., Shi, Z.: Ocean fertilization by pyrogenic aerosol iron, npj Clim. Atmos. Sci., 4, 30, https://doi.org/10.1038/s41612-021-00185-8, 2021.

Jeong, G. Y., Achterberg, E. P.: Chemistry and mineralogy of clay minerals in Asian and Saharan dusts and the implications for iron supply to the oceans. Atmos. Chem. Phys., 14, 12415–12428, https://doi.org/10.5194/acp-14-12415-2014, 2014.

Jeong, G. Y., Nousiainen, T.: TEM analysis of the internal structures and mineralogy of Asian dust particles and the implications for optical modeling, Atmos. Chem. Phys. 14, 7233–7254, https://doi.org/10.5194/acp-14-7233-2014, 2014.

Jeong, G. Y.: Mineralogy and geochemistry of Asian dust: dependence on migration path, fractionation, and reactions with polluted air, Atmos. Chem. Phys., 20, 7411–7428, https://doi.org/10.5194/acp-20-7411-2020, 2020.

Jickells, T. D., An, Z. S., Andersen, K. K., Baker, A. R., Bergametti, G., Brooks, N., Cao, J. J., Boyd, P. W., Duce, R. A., Hunter, K. A., Kawahata, H., Kubilay, N., laRoche, J., Liss, P. S., Mahowald, N., Prospero, J. M., Ridgwell, A. J., Tegen, I., and Torres, R.: Global iron connections between desert dust, ocean biogeochemistry, and climate. Science, 308, 67–71, https://doi.org/10.1126/science.1105959, 2005.

Jickells, T. D., Baker, A. R., Chance, R.: Atmospheric transport of trace elements and nutrients to the oceans, Phil. Trans. R. Soc. A, 374, 20150286, http://dx.doi.org/10.1098/rsta.2015.0286, 2016.

Journet, E., Desboeufs, K. V., Caquineau, S., Colin, J. L.: Mineralogy as a critical factor of dust iron solubility, Geophys. Res. Lett., 35, L07805, https://doi.org/10.1029/2007GL031589, 2008.

Kajino, M., Hagino, H., Fujitani, Y., Morikawa, T., Fukui, T., Onishi, K., Okuda, T., Kajikawa, T., Igarashi, Y.: Modeling transition metals in East Asia and Japan and its emission sources, GeoHealth, 4, e2020GH00259, https://doi.org/10.1029/2020GH000259, 2020.

Kakavas, S., Patoulias, D., Zakoura, M., Nenes, A., Pandis, S. N.: Size-resolved aerosol pH over Europe during summer, Atmos. Chem. Phys., 21, 799–811, https://doi.org/10.5194/acp-21-799-2021, 2021.

Karydis, V. A., Tsimpidi, A. P., Pozzer, A., Astitha, M., Lelieveld, J.: Effect of mineral dust on global atmospheric nitrate concentrations, Atmos. Chem. Phys., 16, 1491–1509, https://doi.org/10.5194/acp-16-1491-2016, 2016.

Kim, A. G., Kazonich, G., Dahlberg, M.: Relative solubility of cations in class F fly ash, Environ. Sci. Technol., 37, 4507–4511, https://doi.org/10.1021/es0263691, 2003.

Kodama, H., Schnitzer, M.: Dissolution of chlorite minerals by fulvic acid, Can. J. Soil Sci., 53, 240–243, https://doi.org/10.4141/cjss73-036, 1973.

Komonweeraket, K., Cetin, B., Aydilek, A. H., Benson, C. H., Edil, T. B.: Effects of pH on the leaching mechanisms of elements from fly ash mixed soils, Fuel, 140, 788–802, http://dx.doi.org/10.1016/j.fuel.2014.09.068, 2015.

Kukier, U., Ishak, C. F., Sumner, M. E., Miller, W. P.: Composition and element solubility of magnetic and non-magnetic fly ash fractions, Environ. Pollut., 123, 255–266, https://doi.org/10.1016/S0269-7491(02)00376-7, 2003.

Kurisu, M., Adachi, K., Sakata, K., and Takahashi, Y.: Stable isotope ratios of combustion iron produced by evaporation in a steel plant, ACS Earth Space Chem., 3, 588–598, https://doi.org/10.1021/acsearthspacechem.8b00171, 2019.

Kurisu, M., Sakata, K., Miyamoto, C., Takaku, Y., Iizuka, T., Takahashi, Y.: Variation of iron isotope ratios in anthropogenic materials emitted through combustion processes, Chem. Lett., 45, 970–972, https://doi.org/10.1246/cl.160451, 2016b.

Kurisu, M., Sakata, K., Uematsu, M., Ito, A., and Takahashi, Y.: Contribution of combustion Fe in marine aerosols over the northwestern Pacific estimated by Fe stable isotope ratios, Atmos. Chem. Phys., 21, 16027–16050, https://doi.org/10.5194/acp-21-16027-2021, 2021.

Kurisu, M., Takahashi, Y., Iizuka, T., and Uematsu, M.: Very low isotope ratio of iron in fien aerosols related to its contribution to the surface ocean, J. Geophys. Res. Atmos., 121, 11119–11136, https://doi.org/10.1002/2016JD024957, 2016a.

Li, R., Zhang, H., Wang, F., He, Y., Huang, C., Luo, L., Dong, S, Jia, X., Tang, M.: Mass fractions, solubility, speciation and isotopic compositions of iron in coal and municipal waste fly ash, Sci. Total Environ., 838, 155974, http://dx.doi.org/10.1016/j.scitotenv.2022.155974, 2022.

Li, S., Zhang, B., Wu, D., Li, Z., Chu, S. Q., Ding, X., Tang, X., Chen, J., Li, Q.: Magnetic particles unintentionally emitted from anthropogenic sources: Iron and steel plants, Environ. Sci. Technol., Lett., 8, 295–300, https://doi.org/10.1021/acs.estlett.1c00164, 2021.

Li, W., Xu, L., Liu, X., Zhang, J., Lin, Y., Yao, X., Gao, H., Zhang, D., Chen, J., Wang, W., Harrison, R. M., Zhang, X., Shao, L., Fu, P., Nenes, A., and Shi, Z.: Air pollution-aerosol interactions produce more bioavailable iron for ocean ecosystems. Sci. Adv., 3, e1601749, https://doi.org/10.1126/sciadv.1601749, 2017.

Lin, Q., Bi, X., Zhang, G., Yang, Y., Peng, L., Lian, X., Fu, Y., Li, M., Chen, D., Miller, M., Ou, J., Tang, M., Wang, X., Peng, P., Sheng, G., Zhou, Z. In-cloud formation of secondary species in iron-containing particles, Atmos. Chem. Phys., 19, 1195–1206, https://doi.org/10.5194/acp-19-1195-2019, 2019.

Liu, L., Li, W., Lin, Q., Wang, Y., Zhang, J., Zhu, Y., Yuan, Q., Zhou, S., Zhang, D., Baldo, C., Shi, Z.: Size-dependent aerosol iron solubility in an urban atmosphere, NPJ Clim. Atmos. Sci., 5, 54, https://doi.org/10.1038/s41612-022-00277-z, 2022.

Liu, L., Zhang, J., Xu, L., Yuan, Q., Chen, J., Shi, Z., Sun, Y., Fu, P., Wang, Z., Zhang, D., Li, W.: Cloud scavenging of anthropogenic refractory particles at a mountain site in North China, Atmos. Chem. Phys., 18, 14681–14693, https://doi.org/10.5194/acp-18-14681-2018, 2018.

Liu, X., Turner, J. R., Hand, J. L., Schichtel, B. A., Martin, R. V.: A global-scale mineral dust equation, J. Geophys. Res. Atmos., 127, e2022JD036937, https://doi.org/10.1029/2022JD036937, 2022.

Lowson, R. T., Comarmond, J., Rajaratnam, G., Brown, P. L.: The kinetics of the dissolution of chlorite as a function of pH and at 25ºC, Geochim. Cosmochim. Acta, 69, 1687–1699, https://doi.org/10.1016/j.gca.2004.09.028, 2005.

Mahowald, N. M., Engelstaedter, S., Luo, C., Sealy, A., Artaxo, P., Benitez-Nelson, C., Bonnet, S., Chen, Y., Chuang, P. Y., Cohen, D. D., Dulac, F., Herut, B., Johansen, A. M., Kubilay, N., Losno, R., Maenhaut, W., Paytan, A., Prospero, J. M., Shank, L. M., Siefert, R. L.: Atmospheric iron deposition: Global distribution, variability and human perturbations. Annu. Rev. Mar. Sci. 1, 245–278, https://doi.org/10.1146/annurev.marine.010908.163727, 2009.

Mahowald, N. M., Hamilton, D. S., Mackey, K. R. M., Moore, J. K., Baker, A. R., Scanza, R. A. and Zhang, Y.: Aerosol trace metal leaching and impacts on marine microorganisms, Nat. Commun., 9(1), 1–15, https://doi.org/10.1038/s41467-018-04970-7, 2018.

Marcotte, A. R., Anbar, A. D., Majestic, B. J., Herckes, P.: Mineral dust and iron solubility: Effects of composition, particles size, and surface area, Atmos., 11, 533, https://doi.org/10.3390/atmos11050533, 2020.

Martin, J. H., and Fitzwater, S. E.: Iron deficiency limits phytoplankton growth in the north-west Pacific subarctic, Nature, 331, 341–343, https://doi.org/10.1126/science.1105959, 1988.

Martin, J. H., Coale, K. H., Johnson, K. S., Fitzwater, S. E., Gordon, R. M., Tanner, S. J., Hunter, C. N., Elrod, V. A., Nowicki, J. L., Coley, T. L., Barber, R. T., Lindley, S., Watson, A. J., van Scoy, K., Law, C. S., Liddicoat, M. I., Lng, R., Stanton, T., Stockel, J., Collings, C., Anderson, A., Bidigare, R., Ondrusek, M., Latasa, M., Millero, F. J., Lee, K., Yao, W., Zhang, J. Z. Friederich, G., Sakamoto, C., Chavez, F., Buck, K., Kolber, Z., Greene, R., Falkowski, P., Chisholm, S. W., Hoge, F., Swift, R., Yungel, J., Turner, S., Nightingale, P., Hatton, A., Liss, P., Tindale, N. W. Testing the iron hypothesis in ecosystems of the equatorial Pacific Ocean. Nature, 371, 123–129, https://doi.org/10.1038/371123a0, 1994.

Martin, J. H.: Glacial-interglacial CO_2 change: The iron hypothesis, Paleoceanogr., 5, 1, 1–13, https://doi.org/10.1029/PA005i001p00001, 1990.

Martínez-García, A., Rosell-Melé, A., Geibert, W., Gersonde, R., Masqué, P., Gaspari, V., Barbante, C.: Links between iron supply, marine productivity, sea surface temperature, and CO_2, over the last 1.1 Ma, Paleoceanogr., 24, PA1207, https://doi.org/10.1029/2008PA001657, 2009.

Martínez-García, A., Rosell-Melé, A., Jaccard, S. L., Geibert, W., Sigman, D. M., Haug, G. H.: Southern Ocean dust-climate coupling over the past four million years, Nature, 476, 312–316, https://doi.org/10.1038/nature10310, 2011.

Martínez-García, A., Sigman, D. M., Ren, H., Anderson, R. F., Straub, M., Hodell, D. A., Jaccard, S. L., Eglinton, T. I., Haug, G. H.: Iron fertilization of the subantarctic Ocean during the last ice age. Science, 343, 1347–1350, https://doi.org/10.1126/science.1246848, 2014.

McDaniel, M. F. M., Ingall, E. D., Morton, Castorina, E., Weber, R. J., Shelley, R. U., Landing, W. M., Longo, A. F., Feng, Y., Lai, B.: Relationship between atmospheric aerosol mineral surface area and iron solubility, ACS Earth Space Chem., 3, 2443–2451, https://doi.org/10.1021/acsearthspacechem.9b00152, 2019.

Moore, C. M., Mills, M. M., Arrigo, K. R., Berman-Frank, I., Bopp, L., Boyd, P. W., Galbraith, E. D., Geider, R. J., Guieu, C., Jaccard, S. L., Jickells, T. D., La Roche, J., Lenton, T. M., Mahowald, N. M., Marañón, E., Marinov, I., Moore, J. K., Nakatsuka, T., Oschlies, A., Saito, M. A., Thingsted, T. F., Tsuda, A., and Ulloa, O.: Processes and patterns of oceanic nutrient limitation, Nature Geosci., 6, 701–710, https://doi.org/10.1038/ngeo1765, 2013.

Nishikawa, M., Batdorj, D., Ukachi, M., Onishi, K., Nagano, K., Mori, I., Matsui, I. and Sano, T.: Preparation and chemical characterisation of an Asian mineral dust certified reference material. Anal. Method., 5, 4088–4095, https://doi.org/10.1039/C3AY40435H, 2013.

Nozaki, Y.: Elemental Distribution, in: Encyclopedia of Ocean Sciences, edited by: Steele, J. H., Thorpe, S. A., and Turekian, K. K., Academic, San Diego, Encyclopedia of Ocean Sciences, 840–845, https://doi.org/10.1006/rwos.2001.0402, 2001.

Nriagu, J. O., and Pacyna, J. M.: Quantitative assessment of worldwide contamination of air, water and soils by trace metals, Nature, 333, 134–139, https://doi.org/10.1038/333134a0, 1988.

Oakes, M., Ingall, E. D., Lai, B., Shafer, M. M., Hays, M. D., Liu, Z. G., Russell, A. G., Weber, R. J.: Iron solubility related to particle sulfur content in source emission and ambient fine particles, Environ. Sci. Technol., 46, 6637–6644, https://doi.org/10.1021/es300701c, 2012.

Pacyna, J. M., Pacyna, E.G.: An Assessment of Global and Regional Emissions of Trace Metals to the Atmosphere from Anthropogenic Sources Worldwide. Environmental Research, 9, 269-298, https://doi.org/10.1139/a01-012, 2001.

Paris, R. and Desboeufs, K. V.: Effect of atmospheric organic complexation on iron-bearing dust solubility, Atmos. Chem. Phys., 13, 4895–4905, https://doi.org/10.5194/acp-134895-2013, 2013.

Praharaj, T., Powell, M. A., Hart, B. R., Tripathy, S.: Leachability of elements from sub-bituminous coal fly ash from India. Environ. Int., 27, 609–615, https://doi.org/10.1016/S0160-4120(01)00118-0, 2002.

Pye, H. O. T., Nenes, A., Alexander, B., Ault, A. P., Barth, M. C., Clegg, S. L., Collett Jr., J. L., Fahey, K. M., Hennigan, C. J., Herrmann, H., Kanakidou, M., Kelly, J. T., Ku, I. T., McNeill, V. F., Riemer, N., Schaefer, T., Shi, G., Tilgner, A., Walker, J. T., Wang, T., Weber, R., Xing, J., Zaveri, R. A., Zuend, A.: The acidity of atmospheric particles and clouds. Atmos. Chem. Phys., 20, 4809–4888, https://doi.org/10.5194/acp-20-4809-2020, 2020.

Rivera. N., Kaur, N., Hesterberg, D., Ward, C. R., Austin, R. E., Duckworth, O. W.: Chemical composition, speciation and elemental associations in coal fly ash samples related to the Kingston ash spill, Energy Fuels, 29, 954–967, https://doi.org/10.1021/ef501258m, 2015.

Sakata, K., Kurisu, M., Takeichi, Y., Sakaguchi, A., Tanimoto, H., Tamenori, Y., Matsuki, A., Takahashi, Y.: Iron (Fe) speciation in size-fractionated aerosol particles in the Pacific Ocean: The role of orgnaic complexation of Fe with humic-like substances in controlling Fe solubility, Atmos. Chem. Phys., 22, 9461–9482, https://doi.org/10.5194/acp-22-9461-2022, 2022.

Sakata, K., Kurisu, M., Tanimoto, H., Sakaguchi, A., Uematsu, M., Miyamoto, C., and Takahashi, Y.: Custom-made PTFE filters for ultra-clean size-fractionated aerosol sampling for trace metals, Mar. Chem., 206, 100–108, https://doi.org/10.1016/j.marchem.2018.09.009, 2018.

Sakata, K., Sakaguchi, A., Yokoyama, Y., Terada, Y., Takahashi, Y.: Lead speciation studies on coarse and fine aerosol particles by bulk and micro X-ray absorption fine structure spectroscopy. Geochem. J., 51, 215–225, https://doi.org/10.2343/geochemj.2.0456, 2017.

Sakata, K., Sakaguhci, A., Tanimizu, M., Takaku, Y., Yokoyama, Y., and Takahashi, Y.: Identification of sources of lead in the atmosphere using X-ray absorption near-edge structure (XANES) spectroscopy, J. Environ. Sci., 26, 343–352, https://doi.org/10.1016/S1001-0742(13)60430-1, 2014.

Sakata, M., Kurata, M., Tanaka, N.: Estimating contribution from municipal solid waste incineration to trace metal concentrations in Japanese urban atmosphere using lead as a marker element, Geochem. J., 34, 23–32, https://doi.org/10.2343/geochemj.34.23, 2000.

Schlitzer, R.: Ocean Data View, https://odv.awi.de (last access: 4 November 2022), 2021.

Schroth, A. W., Crusius, J., Sholkovitz, E. R., and Bostick, B. C.: Iron solubility driven by speciation in dust sources to the ocean, Nature Geosci., 2, 337–340, https://doi.org/10.1038/ngeo501, 2009.

Sedwick, P. N., SHolkovitz, E. R., Church, T. M.: Impact of anthropogenic combustion emissions on the fractional solubility of aerosol iron: Evidence from the Sargasso Sea, Geochem. Geophys. Geosyst., 8, Q10Q06, https://doi.org/10.1029/2007GC001586, 2007.

Seidel, A., Zimmels, Y.: Mechanism and kinetics of aluminium and iron leaching from coal fly ash by sulfuric acid. Chem. Eng. Sci., 53, 3535–3852, https://doi.org/10.1016/S0009-2509(98)00201-2, 1998.

Shah, V., Jacob, D. J., Moch, J. M., Wang, X., Zhai, S.: Global modelling of cloud water acidity, precipitation acidity, and acid inputs to ecosystems, Atmos. Chem. Phys., 20, https://doi.org/10.5194/acp-20-12223-2020, 2020.

Shelley, R. U., Landing, W. M., Ussher, S. J., Planquette, H., and Sarthou, G.: Regional trends in the fractional solubility of Fe and other metals from North Atlantic aerosols (GEOTRACES cruises GA01 and GA03) following a two-stage leach, Biogeosci., 15, 2271–2288, https://doi.org/10.5194/bg-15-2271-2018, 2018.

Shi, Z. B., Woodhouse, M. T., Carslaw, K. S., Krom, M. D., Mann, G. W., Baker, A. R., Savov, I., Fones, G. R., Brooks, B., Drake, N., Jickell,s T. D., Benning, L. G.: Minor effet of physical size sortign on iron solubilitu of transported minerla dust, Atmos. Chem. Phys., https://doi.org/10.5194/acp-11-8459-2011, 11, 8459–8469, 2011.

Sholkovitz, E. R., Sedwick, P. N., and Chrch, T. M.: Influence of anthropogenic combustion emissions on the deposition of soluble aerosol iron to the ocean: Empirical estimates for island sites in the North Atlantic, Geochim. Csmochim. Acta, 73, 14, 3981–4003, https://doi.org/10.1016/j.gca.2009.04.029, 2009.

Sholkovitz, E. R., Sedwick, P. N., Church, T. M., Baker, A. R., Powell, C. F.: Fractional solubility of aerosol iron: Synthesis of a global-scale data set, Geochim. Cosmochim. Acta, 89, 173–189, http://dx.doi.org/10.1016/j.gca.2012.04.022, 2012.

Shupert, L. A., Ebbs, S. D., Lawrence, J., Gibson, D. J., Filip, P.: Dissolution of copper and iron from automotive brake pad wear debris enhances growth and accumulation by the invasive macrophyte *Salvinia molesta* Mitchell, Chemosphere, 92, 45–51, http://dx.doi.org/10.1016/j.chemosphere.2013.03.002, 2013.

Song, Q., Osada, K.: Seasonal variation of aerosol acidity in Nagoya, Japan and factors affecting it, Atmos. Environ., 5, 200062, https://doi.org/10.1016/j.aeaoa.2020.100062, 2020.

Stein, A. F., Draxler, R. R., Rolph, G. D., Stunder, B. J. B., Cohen, M. D. and Ngan, F.: Noaa's hysplit atmospheric transport and dispersion modeling system, Bull. Am. Meteorol. Soc., 96, 2059–2077, https://doi.org/10.1175/BAMS-D-14-00110.1, 2015.

Sullivan, R. C., Guazzotti, S. A., Sodeman, D. A., and Prather, K. A.: Direct observations of the atmospheric processing of Asian mineral dust, Atmos. Chem. Phys., 7, 1213–1236, https://doi.org/10.5194/acp-7-1213-2007, 2007.

Tagliabue, A., Bowie, A. R., Boyd, P. W., Buck, K. N., Johnson, K. S., Saito, M. A.: The integral role of iron in ocean biogeochemistry, Nature, 543, 51–59, https://doi.org/10.1038/nature21058, 2017.

Takahashi Y, Furukawa, T., Kanai, Y., Uematsu, M., Zheng, G., Marcus, M. A.: Seasonal changes in Fe species and soluble Fe concentration in the atmosphere in the Northwest Pacific region based on the analysis of aerosols collected in Tsukuba, Japan, Atmos. Chem. Phys., 13, 7695–7710, https://doi.org/10.5194/acp-13-7695-2013, 2013.

Takahashi, Y., Higashi, M., Furukawa, T., and Mitsunobu, S.: Change of iron species and iron solubility in Asian dust during the long-range transport from western China to Japan, Atmos. Chem. Phys., 11, 11237–11252, https://doi.org/10.5194/acp-11-11237-2011, 2011.

Tao, Y., Murphy, J. G.: The mechanisms responsible for the interactions among oxalate, pH, and Fe dissolution in $PM_{2.5}$, ACS Earth Space Chem., 3, 2259–2265, https://doi.org/10.1021/acsearthspacechem.9b00172, 2019b.

Tao, Y., Murphy, J. G.: The sensitivity of $PM_{2.5}$ acidity to meteorological parameters and chemical composition changes: 10-year records from six Canadian monitoring sites, Atmos. Chem. Phys., 19, 9309–9320, https://doi.org/10.5194/acp-19-9309-2019, 2019a.

Taylor, S. R.: Abundance of chemical elements in the continental crust: a new table, https://doi.org/10.1016/0016-7037(64)90129-2, Geochim. Cosmochim. Acta, 28, 1273–1285, 1964.

Tian., S., Pan, Y., Liu, Z., Wen, T., Wang, Y.: Size-resolved aerosol chemical analysis of extreme haze pollution events during early 2013 in urban Beijing, China, https://doi.org/10.1016/j.jhazmat.2014.07.023, J. Hazard. Mater, 279, 452-460, 2014.

Uno, I., Stake, S., Carmichael, G. R., Tang, Y., Wang, Z., Takemura, T., Sugimoto, N., Shimizu, A., Murayama, T., Cahill, T. A., Cliff, S., Uematsu, M., Ohta, S., Quinn, P. K., Bates, T. S.: Numerical study of Asian dust transport during the springtime of 2001 simulated with the Chemical Weather Forecasting System (CFORS) model, J. Geophys. Res., 109, D19S24, https://doi.org/10.1029/2003JD004222, 2004.

Wåhlin, P., Berkowicz, R., Palmgren, F.: Characterisation of traffic-generated particulate matter in Copenhagen, Atmos. Environ., 40, 2151–2159, https://doi.org/10.1016/j.atmosenv.2005.11.049, 2006.

Wang, Y.S., Yao, L., Wang, L.L., Liu, Z.R., Ji, D.S., Tang, G.Q., Zhang, J., Sun, Y., Hu, B., Xin, J. Y.: Mechanism for the formation of the January 2013 heavy haze pollution episode over central and eastern China, Sci. China Earth Sci., 57, 1, 14-25, https://doi.org/10.1007/s11430-013-4773-4, 2014.

Wang, Z., Fu, H., Zhang, L., Song, W., and Chen, J.: Ligand-promoted photoreductive dissolution of goethite by atmospheric low-molecular dicarboxylates, J. Phys. Chem. A, 121, 16471656, https://doi.org/10.1021/acs.jpca.6b09160, 2017.

Wang, Z., Wang, T., Fu, H., Zhang, L., Tang, M., George, C., Grassian, V. H., Chen, J.: Enhanced heterogeneous uptake of sulfur dioxide on mineral particles through modification of iron speciation during simulated cloud processing, Atmos. Chem. Phys., 19, https://doi.org/10.5194/acp-19-12569-2019, 2019.

Zhang, H., Li, R., Dong, S., Wang, F., Zhu, Y., Meng, H., Huang, C., Ren, Y., Wang, X., Hu, X., Li, T., Peng, C., Zhang, G., Xue, L., Wang, X., Tang, M.: Abundance and fractional solubility of aerosol iron during winter at a coastal city in Northern China: Similarities and contrasts between fine and coarse particles J. Geophys. Res. Atmos.,127, e2021JD036070, https://doi.org/10.1029/2021JD036070, 2022.

Zhang, H., Li, R., Huang, C., Li, X., Dong, S., Wang, F., Li, T., Chen, Y., Zhang, G., Ren, Y., Chen, Q., Huang, R. J, Chen, S., Xue, T., Wang, X., Tang, M.: Seasonal variation of aerosol iron solubility in coarse and fine particles at an inland city in northwestern China, Atmos. Chem. Phys., 23, 3543–3559, https://doi.org/10.5194/acp-23-3543-2023, 2023.

Zhang, L., Wang, Q., Sata, A., Ninomiya, Y., Yamashita, T.: Interactions among inherent minerals during coal combustion and their impacts on the emission of PM_{10}. 2. Emission of submicrometer-sized particles, Energy Fuels, 21, 766–777, https://doi.org/10.1021/ef060308x, 2007.

Zhu, Q., Liu, Y., Shao, T., Tang, Y.: Transport of Asian aerosols to the Pacific Ocean, Atmos. Res., 234, 104735, https://doi.org/10.1016/j.atmosres.2019.104735, 2020.

Zhu, Y., Li, W., Lin, Q., Yuan, Q., Liu, L., Zhang, J., Zhang, Y., Shao, L., Niu, H., Yang, S., Shi, Z.: Iron solubility in fine particles associated with secondary acidic aerosols in east China, Environ. Pollut., 264, 114769, https://doi.org/10.1016/j.envpol.2020.114769, 2020.

Zhu, Y., Li, W., Wang, Y., Zhang, J., Liu, L., Xu, L., Xu, J., Shi, J., Shao, L., Fu, P., Zhang, D., Shi, Z.: Sources and processes of iron aerosols in a megacity in Eastern China, Atmos. Chem. Phys., 22, 2191–2202, https://doi.org/10.5194/acp-22-2191-2022, 2022.

Zuo, P., Huang, Y., Liu, P., Zhang, J., Yang, H., Liu, L., Bi, J., Lu, D., Zhang, Q., Liu, Q., Jiang, G.: Stable iron isotopic signature reveals multiple sources of magnetic particulate matter in the 2021 Beijing sandstorms, Environ. Sci. Technol. Lett., 9, 299–305, https://doi.org/10.1021/acs.estlett.2c00144, 2022.